An early Miocene skeleton of *Brachydiceratherium* Lavocat, 1951 (Mammalia, Perissodactyla) from the Baikal area, Russia, and a revised phylogeny of Eurasian teleoceratines

Alexander Sizov[a, b], Alexey Klementiev[b] and Pierre-Olivier Antoine[c]

a. Geological Institute of Russian Academy of Science, Pyzhevskii pereulok, 7, bld., 1, Moscow 119017, Russia
b. Institute of the Earth's Crust of the Russian Academy of Sciences, Siberian Branch, Lermontova St., 128, Irkutsk, 664033, Russia.
c. Institut des Sciences de l'Evolution, UMR 5554 Univ Montpellier, CNRS, IRD, Place Eugène Bataillon, 34095 Montpellier cedex 5, France

Abstract. Hippo-like rhinocerotids, or teleoceratines, were a conspicuous component of Holarctic Miocene mammalian faunas, but their phylogenetic relationships are widely under-investigated. Excavations in lower Miocene deposits of the Olkhon Island (Tagay locality, Eastern Siberia; 16–18 Ma) have opened a unique window on the poorly-known early history of the Lake Baikal ecosystems, notably in unearthing a skeleton of the teleoceratine *Brachydiceratherium shanwangense* (Wang, 1965). The concerned remains provide new insights into craniomandibular, dental, and postcranial morpho-anatomy of this elusive species. Comparison to most teleoceratine species described in Eurasia allows for proposing phylogenetic relationships among Teleoceratina through a formal parsimony analysis. *Diaceratherium* Dietrich, 1931, as a monotypic genus (earliest Miocene, Western Europe), is retrieved as the earliest teleoceratine offshoot. Other genera are both plurispecific and monophyletic, with *Prosantorhinus* Heissig, 1974 (early Miocene, Eurasia) and *Teleoceras* Hatcher, 1894 (Miocene, North America) forming the sister clade of the (*Brachypotherium*

Roger, 1904 (Miocene, Old World) plus *Brachydiceratherium* Lavocat, 1951) clade. The latter genus includes eight species spanning the late Oligocene–late Miocene interval in Europe and Asia. All teleoceratine genera but *Diaceratherium* span considerable geographical and stratigraphical ranges, likely related to their ultra-generalist ecological preferences.

Keywords: Rhinocerotidae, *Brachydiceratherium shanwangense*, Tagay, Early Miocene, Siberia, Lake Baikal, phylogeny, biogeographical history.

INTRODUCTION

Although they are nearly extinct today, rhinoceroses were one of the most widespread and successful groups of mammals on all the northern continents for over 40 million years. They have freely circulated between Eurasia and North America since the middle Eocene, and are known from Africa since the early Miocene (e.g., Prothero et al., 1989; Antoine et al., 2003). They have also occupied many different modes of life around the world during their long evolutionary history. They ranged from slender- and long-legged savannah roamers to hippo-like forms that apparently lived along rivers and lakes (Prothero et al., 1989; Antoine, 2002). Most hippo-like rhinocerotids are gathered within teleoceratines, a clade at the tribal to sub-tribal level the phylogenetic relationships of which have never been fully elucidated (Antoine, 2002; Lu et al., 2021). Most teleoceratines had hornless skulls, barrel-shaped bodies, and shortened limb bones adapted to swamps and riversides. Teleoceratines span the late Oligocene–latest Miocene interval in Eurasia (Antoine, in press), the Miocene epoch in Africa (Geraads & Miller, 2013), and the early Miocene–early Pliocene in North and Central America (Prothero, 2005). Most of them are interpreted as browsers (based on both dental morphology and isotopic studies; MacFadden, 1998; Hullot et al., 2021).

In this study, we describe a skeleton of a teleoceratine from lower Miocene deposits from the Olkhon Island, Lake Baikal area, Siberia, identify its species assignment and

compare it to most teleoceratine species described in Eurasia. This in-depth comparison allows for performing a parsimony analysis aiming at retrieving phylogenetic relationships among Eurasian Teleoceratina, and for discussing key events in the historical biogeography of teleoceratine rhinocerotids.

LOCALITY AND GEOLOGICAL SETTINGS

Lake Baikal, located in the Baikal Rift System, is morphologically characterised by three basins (Southern, Central and Northern). The Southern and Central basins are thought to have existed permanently since the Paleogene, whereas the Northern Basin did not develop before the Late Miocene (Mats et al., 2010, 2011). Olkhon Island (Russian: Ольхон) is located in the transitional zone between the Central and the Northern basins of Lake Baikal. It is separated from the mainland in the west by a shallow Maloe More strait (Russian: Малое Мope; in English literally the Small Sea) of the Northern Basin that extends far to the south. In the south, Maloe More strait is connected through the narrow Olkhonskie Vorota strait (Russian: Ольхонские Ворота; in English literally the Olkhon Gate) to the central part of Lake Baikal. From the northwestern part of Olkhon Island, one locality known as Tagay or Tagai (Russian: Тагай or Тогай) has yielded numerous terrestrial fossils of the Neogene (Fig. 1). The Neogene sediments in Tagay Bay belong to the Tagay Formation (Logachev et al, 1964; Mats et al., 2001; Mats, 2013, 2015). Sediments are exposed in the northeastern part of the bay in a steep erosional cliff up to 15 m high. Elsewhere along the shores of the bay, it is levelled by landslides. The cliff borders a large landslide circus and a sandy beach below.

The Tagay locality was discovered in the 1950s (Kitainik & Ivaniev, 1958). First paleontological studies of the large mammals were performed in 1958 under the direction of N.A. Logachev (Logachev et al., 1964). Studies of small mammals had been carried out occasionally by A.G. Pokatilov since the 1970s (Pokatilov, 2004). Tagay preserves an

abundant fossil fauna that includes molluscs and vertebrates such as fish, amphibians, reptiles, birds and mammals. However, a significant part of the paleontological material was determined only tentatively for a long time: Mustelidae, Felidae, *Anchitherium* sp, *Metaschizotherium*(?) sp., and *Dicerorhinus*(?) sp. among perissodactyls, *Palaeomeryx* sp. and Bovidae among artiodactyls (Logachev et al., 1964). Artiodactyl remains were reexamined, which led to the following list: Cervidae (*Amphitragulus boulangeri*, *Lagomeryx parvulus*, *Stephanocemas* sp.), Palaeomerycidae (*Orygotherium tagaiense*, *Palaeomeryx* cf. *kaupi*) and Anthracotheriidae (*Brachyodus intermedius*) (Vislobokova, 1990, 1994, 2004). Chelonians were studied by Khosatzky and Chkhikvadze (1993) and the ichthyofauna by Sytchevskaya (Filippov & Sytchevskaya, 2000). The Neogene sediments were examined based on sedimentological, stratigraphical, and palaeontological aspects by (Kossler, 2003). A new phase of the study of Tagay locality started in 2008. Annual palaeontological studies have been carried out since that year (Rage & Danilov, 2008; Klementiev, 2009; Danilov et al., 2012; Syromyatnikova, 2014, 2015; Tesakov & Lopatin, 2015; Klementiev & Sizov, 2015; Zelenkov, 2016; Sotnikova et al, 2021).

The Tagay Formation consists of alternating beds of clays and clayey sands containing interlayers and lenses of carbonate concretions of diagenetic origin. Deposits rest upon the crystalline basement, submerging below the water to the south. Clay beds are mostly green and brown, sometimes black. There are also lenses and interlayers of brick red and red clay and loam. Bone beds, also accordant to sedimentary cycles, were marked with letters (A, B, C, ... downsection) (Fig. 2 A, B). Most clay beds have predominant ferruginous-magnesian montmorillonites composition. A remarkable feature of clay sediments is the high (up to 8%) content of silt-psammite-psephite admixtures. Moreover, most psammite-psephitic fragments are not rounded and have angular and indented outlines, which indicates their insignificant

transportation. Lithological descriptions of the sections and specification of the bone beds are available in the papers (Logachev et al., 1964; Sizov & Klementiev, 2015).

Neogene continental deposits in the late early Miocene Tagay locality have yielded a diverse vertebrate fauna. The vast majority of unearthed forms are strictly or predominately woodland inhabitants. Taxonomically, the fauna represents a mixture of European, Asian, and North American taxa, and thus is of great importance for intercontinental and pan-Eurasian faunal correlations. Based on the faunal similarity, the Tagay fauna likely correlates with the Shanwangian Mammal Age/Stage of China. According to the views of various specialists, the age of the Tagay Fauna correlates to the interval of units MN3 through MN5 (Rössner & Mörs, 2001; Vislobokova, 2004; Klementiev & Sizov, 2015; Sotnikova et al., 2021). Conversely, some other researchers have correlated the Tagay fauna with the European Mammal Zone MN 7+8 and the Chinese Mammal Unit NMU7~~, which we think is wrong~~ (Daxner-Höck et al., 2013) (Fig. 1 B).

MATERIAL AND METHODS

All the remains described here belong to a single adult individual (IZK79-1-08C-1/), stored in the collection of the Institute of the Earth's Crust (Irkutsk, Russia). Alexey Klementiev and Gennady Turkin at Tagay site discovered this skeleton in 2008 (Fig. 2 B, C) (Klementiev, 2009).

Capital letters are used for upper teeth (I, C, D, P, M), and lower-case letters for lower teeth (i, c, d, p, m). Dental terminology is that of Heissig (1972: pl. 13) and Antoine (2002) for rhinocerotids. Anatomical features described follow basically the same sequence as in Antoine (2002), and Antoine et al. (2010). The sequence of described dental and osteological features follows Antoine (2002). Rhinocerotid dental terminology follows Heissig (1969) and Antoine (2002), while dental and skeletal measurements were taken according to Guérin

(1980). Dimensions are given in mm. The locomotion type is based on the gracility index of the McIII and MtIII (100 × TDdia/L; Guérin, 1980).

The stratigraphical framework is based on geological time scales and European Land Mammal Ages for the Neogene (Hilgen, Lourense & Van Dam, 2012; Raffi et al, 2020).

3D-rendering

All significant bones of the rhinoceros were scanned with a resolution of 0.25 mm using a RangeVision Smart - a 3D scanner, working on the principle of structured illumination. RangeVision Smart has three areas of scanning and is equipped with colour cameras 1.3 Mpix and is equipped with a specially designed software RangeVision 2020.2 which we used for visualization, segmentation and 3D rendering. RangeVision 2020.2 allows to get a ready-made 3D model of high quality for further work in all popular CAD/CAM programs and virtual 3D modelling environments (Solidworks, Autocad, 3DS Max, Maya, Rhinoceros and other), providing formats ".obj" , ".stl", ".ply" etc.

Parsimony analysis

The parsimony analysis was performed through 282 cranio-mandibular, dental, and postcranial characters primarily derived from those of Antoine (2002, 2003) and scored on 31 ceratomorph species (i.e., one tapirid plus 30 rhinocerotoids). All multistate characters were treated as additive, except for the characters 72, 94, 102, 140, and 187 (non-additive).

The outgroup includes the living Brazilian tapir *Tapirus terrestris* (Linnaeus, 1758), the Eocene non-rhinocerotid rhinocerotoid *Hyrachyus eximius* Leidy, 1871 and the Paleogene stem rhinocerotids *Trigonias osborni* Lucas, 1900 (Eocene of North America) and *Ronzotherium filholi* (Osborn, 1900) (Oligocene of Western Europe). Aside from the outgroup, we have included a branching group (Antoine, 2002, 2003; Orliac et al., 2010; Boivin et al., 2019), consisting of 12 species classically assigned to all suprageneric groups

but Teleoceratina among Rhinocerotinae, and aimed at i) further testing the monophyly of the in-group and ii) replacing it among Rhinocerotinae. The branching group includes an early-diverging representative of Rhinocerotinae (*Plesiaceratherium mirallesi* (Crusafont, Villalta & Truyols, 1955)), three species among Aceratheriini (*Aceratherium incisivum* Kaup, 1832, *Acerorhinus zernowi* (Borissiak, 1914), and *Alicornops simorrense* (Lartet, 1851)), and eight members of the Rhinocerotina, encompassing all five living rhinoceroses, namely the Indian rhino (*Rhinoceros unicornis* Linnaeus, 1758), the Javan rhino (*Rhinoceros sondaicus* Desmarest, 1822), the Sumatran rhino (*Dicerorhinus sumatrensis* (Fischer, 1814)), the white rhino (*Ceratotherium simum* (Burchell, 1817)), and the black rhino (*Diceros bicornis* (Linnaeus, 1758)), but also three fossil species: *Lartetotherium sansaniense* (Miocene of Europe; Heissig, 2012), *Gaindatherium browni* Colbert, 1934 (Miocene of South Asia; Heissig, 1972 ; Antoine, in press), and *Nesorhinus philippinensis* (Von Koenigswald, 1956) (early Middle Pleistocene of the Philippines; Antoine et al., 2022 and references therein).

The ingroup sensu stricto (Teleoceratina) comprises 15 terminals, with *Teleoceras fossiger* Cope, 1878 (late Miocene to earliest Pliocene, North America), *Brachypotherium brachypus* (Lartet in Laurillard, 1848) (late early and middle Miocene, Eurasia), *Brachypotherium perimense* (Falconer & Cautley, 1847) (Miocene, South Asia), *Prosantorhinus germanicus* (Wang, 1929) (late early and middle Miocene, Europe), *Prosantorhinus douvillei* (Osborn, 1900) (late early and early middle Miocene, Europe), *Prosantorhinus laubei* Heissig & Fejfar, 2007 (early Miocene, central Europe), and a comprehensive sample of terminals either classically or more recently assigned to *Diaceratherium* Dietrich, 1931. They consist of the type species *D. tomerdingense* Dietrich, 1931 from the earliest Miocene of Tomerdingen (Germany), *D. lemanense* (Pomel, 1853) from the latest Oligocene-early Miocene of Western Europe (also described under the *Diceratherium* (*Brachydiceratherium*) *lemanense* combination by Lavocat, 1951), *D.*

aurelianense (Nouel, 1866) from the early Miocene of Western Europe, *D. asphaltense* (Depéret & Douxami, 1902) from the earliest Miocene of Western Europe, *D. fatehjangense* (Pilgrim, 1910), from the Miocene of Pakistan and early Miocene of Kazakhstan (previously described as "*Brachypotherium aurelianense* Nouel, var. nov. *Gailiti*" by Borissiak, 1927), *D. aginense* (Répelin, 1917) from the earliest Miocene of Western Europe, *D. shanwangense* (Wang, 1965) from the late early Miocene of eastern China (Shanwang; Lu et al., 2021), Japan, and eastern Siberia (Tagay; this work), and *D. lamilloquense* Michel, in Brunet et al., 1987 from the late Oligocene of France. *Aceratherium gajense intermedium* Lydekker, 1884 has disputed taxonomic affinities. Even if it has been subsequently assigned to the aceratheriine genera *Subchilotherium* (e.g., Heissig, 1972) or *Chilotherium* (e.g., Khan et al., 2011), Antoine et al. (2003) considered that this taxon might document a teleoceratine instead, although of uncertain generic assignment, based on a parsimony analysis taking into account the holotype and original hypodigm. The recognition of associated dental and postcranial remains from the Potwar Plateau (late early to early late Miocene, Pakistan) allowed for defining the new combination *Diaceratherium intermedium* (Lydekker, 1884), as recently proposed by Antoine (in press). This debated taxonomic issue will be tested here.

Three indisputable representatives of Teleoceratina, such as *Diaceratherium* cf. *lamilloquense* from the late Oligocene of Thailand (Marivaux et al., 2004), *Brachypotherium gajense* (Pilgrim, 1910), from the late Oligocene–earliest Miocene of Pakistan, and *Prosantorhinus shahbazi* (Pilgrim, 1910), from the early Miocene of Pakistan (combinations proposed by Antoine et al., 2010 and Antoine, in press) were not included in the analysis, due to their very partial hypodigms, restricted to a few elements likely to blur the phylogenetic signal and to generate much uncertainty in the analysis.

Moreover, *Diaceratherium askazansorense* Kordikova, 2001 from the early Miocene of Kazakhstan was not included either, as dental and postcranial elements assigned to this taxon

closely resemble those of *Pleuroceros blanfordi*, a stem member of Rhinocerotinae (early Miocene of South Asia; Antoine et al., 2010; Prieto et al., 2018) and, to a lesser extent, of *Pleuroceros pleuroceros* (earliest Miocene of western Europe; Antoine et al., 2010; Antoine & Becker, 2013). Similarly, the early late Oligocene species *Diaceratherium massiliae* Ménouret & Guérin, 2009 was recently shown to be a junior synonym of the short-limbed and early-diverging rhinocerotid *Ronzotherium romani* Kretzoi, 1940, through a thorough re-examination of most available material and the recognition of new associated dental and postcranial specimens in Switzerland (Tissier et al., 2021). Hence, it was not considered in the present phylogenetic analysis.

The parsimony analyses were performed through the heuristic search of PAUP 4 3.99.169.0 (Swofford, 2002), with tree-bissection-reconnection (reconnection limit = 8), 1000 replications with random addition sequence (10 trees held at each step), gaps treated as missing, and no differential weighting or topological constraint a priori.

Systematics

Generic and suprageneric systematics follows the arrangement as supported by the present parsimony analysis (see below).

SYSTEMATIC PALAEONTOLOGY

Order Perissodactyla OWEN, 1848

Family Rhinocerotidae GRAY, 1821

Subfamily Rhinocerotinae GRAY, 1821

Tribe Rhinocerotini GRAY, 1821

Subtribe Teleoceratina HAY, 1902

Genus *Brachydiceratherium* LAVOCAT, 1951

Type species: *Brachydiceratherium lemanense* (Pomel, 1853) by subsequent designation

Referred species: *Brachydiceratherium aurelianense* (Nouel, 1866) from the early Miocene of Western Europe; *Brachydiceratherium intermedium* Lydekker, 1884, from the early–late Miocene of the Indian Subcontinent (Antoine et al., 2013; Antoine, in press); *Brachydiceratherium asphaltense* (Depéret & Douxami, 1902) from the earliest Miocene of Western Europe; *Brachydiceratherium fatehjangense* (Pilgrim, 1910), from the Miocene of Pakistan and early Miocene of Kazakhstan (senior synonym of "*Brachypotherium aurelianense* Nouel, var. nov. *Gailiti*" by Borissiak, 1927); *Brachydiceratherium aginense* (Répelin, 1917) from the earliest Miocene of Western Europe; *Brachydiceratherium shanwangense* (Wang, 1965) from the late early Miocene of eastern China (Shanwang; Lu et al., 2021), Japan, and eastern Siberia (Tagay; this work); *Brachydiceratherium lamilloquense* Michel, in Brunet et al., 1987 from the late Oligocene of France.

Diagnosis: Teleoceratines with a small nuchal tubercle, articular tubercle smooth on the squamosal, with cement present on cheek teeth, protocone always constricted on P3-4, labial cingulum usually absent on lower premolars and always present on lower molars, foramen vertebrale lateralis present and axis-facets transversally concave on the atlas, a postero-distal apophysis low on the tibia, and a latero-distal gutter located posteriorly on the fibula.

Geographical and stratigraphical range: Late Oligocene and/or Miocene of Eurasia, with an early Miocene climax.

Brachydiceratherium shanwangense (Wang, 1965)

Diagnosis: Representative of *Brachydiceratherium* with a lateral apophysis present on the nasals, a median nasal horn present on the nasals, premolar series short with respect to the molar series, roots distinct on the cheek teeth, crochet always simple and lingual cingulum usually absent and always reduced on P2-4, crista always present on P3, protocone strongly constricted on M1-2, lingual cingulum usually absent on lower premolars and always absent on lower molars, d1/p1 absent in adults, glenoid fossa with a medial border straight on the scapula, distal gutter absent on the lateral epicondyle of the humerus, proximal radius-ulna facets always fused, and trochanter major low on the femur.

Geographical and stratigraphical range: Late early Miocene of the Shanwang Basin, Shandong Province, China (see Lu et al., 2021) and of Irkutsk Region, Russia (Tagay locality, Olkhon Island, Lake Baikal).

Material available: IZK79-1-08C-1, almost complete skeleton, including the skull (occipital, parietal, frontal, the right zygomatic and lacrimal, both nasals, and temporals with processes and also premaxillae), the jaws, most vertebrate and ribs, both humeri, radii and ulnae, both femora, tibiae, right fibula, most metacarpals, and several metatarsals and phalanges. The skeleton described herein was found disarticulated at the junction of layers of sand and clay (Fig 2 B, C). In general, the right side of the individual is much better preserved than is the left.

DESCRIPTION

Skull

The skull (Fig. 3) was found disconnected, but there is no doubt that the separate bones belong to the same individual, because they were found in close proximity to one another with no extraneous elements, and they fit together well. The temporal, zygomatic and lacrimal, nasal, frontal, parietal and occipital fit each other perfectly. The remaining bones are matching in size, colour and texture. The skull is short and relatively wide (Lcondylesnasals = 540 mm, Wfrontals ≈ 190 mm), belonging to a large-sized adult rhinocerotid. The separated nasal bones are long and longer than the premaxilla, relatively thin and bear a lateral apophysis. Roughness for a small nasal horn is preserved at the tip of the nasals. In lateral view, the foramen infraorbitalis and the posterior border of the U-shaped nasal notch are both located above the P3, while the anterior border of the orbit is above the M1. The minimum distance between the posterior edge of the nasal notch and the anterior border of the orbit is 67.2 mm.

Cranial features. The skull was partly destroyed and some elements were reconstructed in anatomical position by one of us (AS). It is short, broad, and elevated. The dorsal profile of the skull is concave, with a small protuberance for a short nasal horn and an upraised parietal bone (50°). In lateral view, the nasals have a small ventrolateral prominence (lateral apophysis, sensu Antoine, 2002). The maxilla is badly damaged and the area of the foramen infraorbitalis is restored on both sides. Nevertheless, based on the preserved part of the maxilla, a position above P4 can be hypothesised. The posterior end of the nasal notch is located above the anterior part of P3. The nasal septum is not ossified at all. The premaxillae are broken rostrally. They form a short and elevated strip, slightly dipping frontward, with a deep ventral sulcus. Relations between nasal and lachrymal bones are not observable, and neither are the lachrymal processi. The anterior border of the orbit is situated above the middle of M1. On the frontal, a pair of smooth tubercles lay on the dorsal and posterodorsal edges of the orbit (processus postorbitalis). The anterior base of the processus zygomaticus

maxillary is low, ~1 cm above the neckline of molars. The zygomatic arch forms a straight, low, and oblique strip, with parallel dorsal and ventral borders. It is parallel to the dorsal outline of the skull, with a rounded and rugose posterodorsal tip. A marked processus postorbitalis deforms the dorsal edge of the zygomatic process, at the junction between the jugal and the squamosal. Its tip, located on the latter bone, has a rugose aspect. Most of the temporal fossa elements are not preserved and it is therefore impossible to consider the shape and relations of the foramina sphenorbitale and rotundum. The area between the temporal and nuchal crests is depressed, forming a deep gutter. The external auditory pseudo-meatus is partly closed ventrally. The posterior side of the processus zygomaticus is flat in lateral view (no posterior groove). The occipital side is inclined up- and forward, with a very salient nuchal tubercle (although small, i.e., not extended on a wide area), determining a diamond-shape to the skull in dorsal view. The occipital condyles are oriented in the same axis as the skull in lateral view. The posterior tip of the tooth row reaches the posterior third of the skull. The pterygoids are not preserved, as most of the basicranium, vomer, and basal foramina. The skull is brachycephalic (interzygomatic width/total length ~0.57). As observable in dorsal view, the nasals have a sharp tip. They are long and unfused, fully separate by a deep groove from tip to tip. There were no lateral nasal horns, but a small median nasal horn, as unambiguously shown by the presence of axial vascularised rugosities in the anterior quarter of the nasal bones. In contrast, the frontal bones have a smooth aspect, thus indicating the absence of a frontal horn. The orbits were not projected laterally. The zygomatic arches are 1.51 times wider than the frontals. From this frontal ambitus, run posteriorly two straight and smooth frontal crests, getting closer by the parietals (minimum distance = mm), and then abruptly diverging and forming an occipital crest concave posteriorly. The transition from the maxilla to the processus zygomaticus maxillary is progressive, with no brutal inflection. The articular tubercle of the squamosal is smooth (in lateral view) and straight (in sagittal view).

The right processus postglenoidalis forms a rounded right dihedron in ventral view. The foramen postglenoideum is remote from the latter. The left one is not preserved. The occipital side is wide and, accordingly, the processus posttympanicus and the processus paraoccipitalis are distant. The former is poorly developed, while the latter is very long, slender, and vertical. The foramen magnum is not well preserved enough for allowing any observation. The occipital condyle has a median ridge but no medial truncation.

Mandible

In lateral view, the symphysis is upraised, with an angular ventral profile determined by two successive inflections. The foramen mentale is widely open and located below p2 (left) and p3 (right). The corpus mandibulae is low, with a straight ventral border. It is getting regularly higher to the mandibular angle, smooth, rounded and hugely developed. There is a shallow vascular incisure. The ramus is low, with a posterior border oblique up- and frontwards and an anterior border vertical. The processus coronoideus is high, tapering dorsally, and somewhat concave posteriorly. The condyloid process is high and sharp-edged, separate from the latter by a deep mandibular notch. In dorsal view, the symphysis is massive, well developed anteroposteriorly and narrow, with i2s and lateral edges parallel and two circular alveoli for small i1s. The posterior border of the symphysis is located between the trigonids of p3. The tooth rows are more parallel than the bodies (Fig. 4), which widely diverge posteriorly. The spatium retromolare is wide on both sides. The mylohyoid sulci are present but very shallow.

The foramen mandibulare opens below the teeth-neck line.

Dental material

The dental formula is 1-0-4-3/2-0-3-3. No decidual dentition is known.

Upper dentition (Fig. 4). The first upper incisors are not preserved, but straight and sagittally-elongated alveoli point to an oval cross section for them (as usual in teleoceratines).

There are no I2, I3, or C. The premolar series is short with respect to the molar series (LP3-4/LM1-3*100=48.7; Lp3-4/Lm1-3*100=45.8), which is further highlighted by the small size of P2 and p2. Enamel is thick, wrinkled and corrugated, and partly covered with a thin layer of cement. Teeth are low crowned, with roots partly joined. The labial cingulum is absent on the upper cheek teeth. A thick paracone fold is present on P2-M3, vanishing with wear on P2-M1 and marked until the neck on M2-3. There is no metacone fold or mesostyle on the upper cheek teeth. Short and wide crochet is present on P3-4 (always simple), but absent on P2. There is no metaloph constriction on P2-4. The lingual cingulum is absent on all upper cheek teeth, except for a small tubercle on the anterolingual base of the hypocone on both P4. The postfossette forms a small and deep isometric pit. The antecrochet is getting stronger backward, from absent on P2 and short on P3-4 to very elongate on M1-3. The first upper cheek tooth is most likely a persistent D1: it is much more worn than other teeth and the enamel is also much thinner. It is preserved on the right side and its presence is further attested by two alveoli on the left side (heart-shaped anterior root; peanut-shaped posterior root). It has a sharp anterolingual cingulum, a straight lingual edge, and rounded posterior and labial edges. P2-4 are fully molariform (bilophodont, with an open lingual valley). On P2, the metaloph is transverse labially, but curved posterolingually due to the position of the hypocone. The latter is much more developed than the protocone. The protoloph is thin but continuous, transversely oriented. There is no medifossette on P3-4, but a short crista on P4 and on P3 (mostly wiped out by wear). The protocone is constricted anteriorly on P3-4. The metaloph forms a dihedron on P3-P4, with the crochet as a tip and the hypocone located posterior to the metacone. The protoloph is complete and continuous and there is no pseudometaloph on P3. The metacone is not constricted or isolated on P3-4. The crochet is long and sagittal on M1-M3, with a rounded tip on M1, and a sharp tip on M2-3. There is no crista, medifossette, or cristella on upper molars. The lingual cingulum is restricted to a small

pair of tubercles on M2s and a smooth ridge on the hypocone of M3. The protocone is strongly constricted on M1-3, and a trefoil shaped on M3. The parastyle is short and sagittal on M1-3; the paracone fold is very salient on M2 and especially on M3. The metastyle is very long on M1-2. The metaloph is almost as long as the protoloph on M1-2. In lingual view, the protocone is increasingly developed sagittally from M1 to M3. A deep groove carves the anterolingual side of the hypocone on M2, and a shallower one is observed on M1. The ectoloph is straight on M1 and concave on M2. The antecrochet and the hypocone are close but separate on M1-2. There is no lingual groove on the lingual side of M2. The posterior cingulum is complete on M1-2 and the postfossette is still narrower and deeper than on premolars. The right M3 has a triangular outline in occlusal view, with a straight ectometaloph (the left M3 is not preserved). The protoloph is transversely developed. There is no posterior groove on the ectometaloph and the labial cingulum is restricted to a low and smooth spur covering the lingual third of the former.

Lower dentition (Fig. 4). There are small circular alveoli for both i1s, between the i2s, in the symphyseal part of the dentary but the shape of the concerned teeth is unknown. The presence of a short p2 is attested by three closely-appressed alveoli on the right side (area unpreserved on the left side), but no d1 or p1 was present, as attested by the sharp ridge running anterior to p2's alveoli. There are no vertical rugosities on the ectolophid of p3. On lower cheek teeth, ectolophid grooves are developed (neither U- or V-shaped) and vanishing before the neck, trigonids are rounded and forming a right angle in occlusal view, metaconids and entoconids are unconstricted. The bottom of the lingual valleys is V-shaped in lingual view on lower premolars. On lower premolars, the lingual cingulum is restricted to a low ridge continuing the anterior cingulum on the trigonid of p3s, and the labial cingulum consists of a small edge obtruding the ectolophid groove on p4s. Lower molars lack a lingual cingulum but a small cingular ridge partly obtrudes the ectolophid groove. The hypolophid is

oblique in occlusal view on m1-3. There is no lingual groove on the entoconid of m2-3. The posterior cingulum of m3 forms a low, horizontal, and transversely-elongated ridge.

Poscranial skeleton

Atlas. The atlas is wide and short sagittally. In dorsal view, the transverse processes (partly broken) and the alar notches are developed and the axis-facets are concave. In anterior view, the rachidian canal has a bulb-like outline. The occipital condylar facets are kidney-like. The foramen vertebralis cuts across the anterior third of the dorsal surface on both sides and it is continued by a shallow groove laterally (for the vertebral artery). In posterior view, the foramen transversarium is present, wide and partly hidden by the lateral expansion of each axis-facet (Fig. 5, A).

Axis. The axis is stocky, with thick and cylindric dens and tear-shaped atlas-facets (convex transversely) on the prezygapophyses. The spinous process is thick and carinated. The foramen vertebrale is large and subtriangular. The postzygapophyses have wide and circular facets for the first thoracic vertebra, forming a ~45° angle with the horizontal line. The centrum is very long anteroposteriorly, with a pentagonal outline in posterior view (Fig. 5, B). Most thoracic vertebrae are preserved. They are massive, with heart-shaped centrums, and stocky transverse processes. The dorsal spines are slender and oblique (45° with the vertical line), with a length reaching up to 250% of the centrum height for the T4-6.

The appendicular skeleton strongly recalls that of recent Sumatran rhinoceroses (*Dicerorhinus sumatrensis*), in terms of size and robustness. The stylopodium is strikingly slender (both the femora and humeri) and there is no noticeable shortening of the autopodium. Nevertheless, the carpus is very low and massive with respect to both more proximal and more distal elements of the arm.

Scapula. The scapulae are partly preserved. They are elongated dorsoventrally, notably due to their anteroposterior narrowness (H/APD = XX). The scapular spine is straight, much

developed and with an extremely salient tuberculum bent caudally. There is no pseudo-acromion. The tuberculum supraglenoidale is well distinct from the cavitas glenoidalis. The medial border of the cavitas glenoidalis is straight, determining a semi-circular outline in ventral view.

Humerus. Both humeri are almost complete (Fig. 6, A-E). The humerus is a slender bone, with a straight diaphysis. The trochiter is high, with a smooth and rounded outline. The caput humeri is wide and rounded, with a rotation axis forming a 40° angle with the vertical line. The deltoid crest is elongated, almost reaching the mid-bone. The deltoid tuberosity is not much salient. The fossa radii is wide and shallow. The fossa olecrani is higher than wide. The distal articulation is egg-cup shaped, without marked median constriction. The trochlea is half-conical and the capitulum humeri is half-cylindrical. There is no synovial fossa ("trochlear scar") on the anterodorsal edge of the trochlea. The lateral epicondyle is elongated dorsoventrally and its ventral border ends dorsal to the capitulum humeri, lacking a distal gutter.

Radius. The two bones are complete and undistorted (Fig. 06, F-J). The anterior border of the proximal articulation is straight in dorsal view but convex in anterior view. The radius is slender, with a distal extremity larger than the proximal one in anterior view. The diaphysis is much slender, especially in its proximal half. It has a straight medial border in anterior view, but it is posterolaterally concave, which determines a wide spatium interosseum brachii when the ulna is in anatomical connection. The proximal ulnar facets are fused on both sides. The insertion of the m. biceps brachii is wide but shallow, with two small pits. Ulna and radius are independent, apart from the proximal and distal articular areas. On the anterodistal part of the diaphysis, the gutter for the m. extensor carpi is not marked at all. There is only one distal facet for the ulna on the lateral side of the bone. The posterior expansion of the

scaphoid-facet is high, determining a right-angled rectangle. There is a wide pyramidal-facet on the distal articulation.

Ulna. The bone is sturdy, with a long and heavy olecranon, the tip of which is wide and diamond shaped (Fig. 6, K-O). The diaphysis is straight, triangular in cross- section and as robust as the radius shaft. It forms a *c.* 135° angle with the olecranon in lateral view. The humeral facet is saddle-shaped. The proximal radio-ulna facets form a continuous pad, with a wide medial strip and a high triangular lateral fact. A smooth but salient anterior tubercle overlooks the distal end of the bone. There is neither a second distal radius-facet on the medial side of the diaphysis nor semilunate-facet on the distal side. The almond-shaped distal radius-facet is separate proximally from a salient horizontal ridge by a deep and rugose depression. The pyramidal-facet is concavo-convex, with a quarter-circle outline in distal view.

The carpus is very low and massive, especially with respect to slender stylopodial and zeugopodial elements. All carpals have salient tubercles on the anterior aspect of the bones. The right hand is more complete than the left one.

Scaphoid. The scaphoid is low and massive, with equal anterior and posterior heights. The proximal radial facet is diamond shaped in proximal view. The posteroproximal semilunate facet is strongly distinct. It is oval, wide, and separated from all other facets. A deep depression hollows the lateral side between the semilunate-facets. The anterodistal semilunate-facet is nearly flat and crescent shaped. The magnum-facet is concave in lateral view. The trapezium-facet is smaller than other distal facets, but it forms a wide triangle, separated from the trapezoid-facet by a smooth ridge.

Semilunate. The bone is compact. In proximal view, the anterior facet only responds to the radius, whereas the wide posteromedial facet is for the scaphoid. The anterior side is smooth (not keeled or carinated), with a sharp distal tip. On the lateral side, both pyramidal-

facets are closely appressed. The proximal one is almond shaped and the distal one is comma like. The posterior tuberosity is short. Most of the distal side is articulated, medially with the magnum and laterally with the unciform.

Pyramidal. The bone is almost cubic. The proximal side is square, with a saddle-shaped ulna-facet. The semilunate-facets are sagittally elongated, with a half-oval outline for the proximal one and a crescent-like shape for the distal one. The pisiform-facet is comma shaped, with a concave sagittal profile and it overhangs a strong lateral tuberosity. The distal facet, for the unciform forms a right isosceles triangle with rounded angles. There is no magnum-facet.

Pisiform. The right pisiform is short, high, and spatulate, with large and triangular radius- and pyramidal-facets. Both facets are separated by a sharp ridge and form a right angle. There is no strong constriction separating the thick body and the articulated part. The medial edge of the body is straight and vertical.

Trapezium. The right trapezium is preserved. It is a small proximo-distally flattened bone with a circular outline in proximal view. The proximal side is almost entirely occupied by a wide pentagonal scaphoid-facet (compatible with the large-sized trapezium-facet on the scaphoids). The latero-distal side bears a right-triangled trapezoid-facet overhanging a deep pit. All other sides have a rugose aspect and they are devoid of articular facets.

Trapezoid. Only the right trapezoid is documented. It is wider than high, almost cubic. Only the anterior and posterior sides (oval and pentagonal in shape, respectively) are free of articular surfaces. The proximal side, saddle shaped and tapering backwards, responds to the scaphoid. In medial view, the trapezium-facet is restricted to the posterior half, with a deep insertion pit located close to the anterior edge. The lateral facet is al low rectangle for the magnum. The distal side, weakly concavo-convex, consists of a pentagonal McII-facet.

Magnum. The magnum has a very low anterior aspect, with a subrectangular outline and a salient horizontally-elongated median pad. The proximal border is straight in anterior view. In medial view, the anteromedial facets are in contact over their length (no anterior groove). In lateral view, the dorsal pulley for the semilunate forms a low-diameter half circle, further determining a question mark proximal profile. The distal facet is wide and tapering posteriorly. The posterior tuberosity is broken on the left magnum, and it is very short on the right specimen.

Unciform. The bone is compact, with a posterior tuberosity wide and much developed sagittally. The anterior side is wide and low, with a pentagonal outline and a maximum height on its lateral tip. The proximal side has two anterior facets flat transversally and convex sagittally, separated by a sharp sagittal edge. The medial one, triangular, is for the semilunate while the lateral one, diamond shaped, is for the pyramidal. The latter has a wide posterolateral expansion joining the lateral edge and the McV-facet (located on the distal side) on the right unciform. This part is broken on the left one. From the medial tip, the distal and distolateral sides have three contiguous facets, responding to the McIII (small and quadrangular), McIV (bulb-shaped), and McV (oval and deeply concave sagittally), respectively. They are only separated by smooth sagittal grooves. The McV-facet is oblique, which could suggest the presence of a functional McV (see Antoine, 2002, 2003; Boada-Saña et al., 2008).

The hand and pes have a mesaxonian Bauplan. Although no McV is preserved, the hand was probably tetradactyl, as hypothesised by the vertical facet on the McIV (see above). The metapodials have salient insertions for the m. extensor carpalis. Their shafts are robust (wide transversally and flattened sagittally), with neither distal widening nor clear shortening (no brachypody; see Antoine, 2002). The insertions for the m. interossei are long, reaching the mid-shaft on all available metapodials. The intermediate reliefs do not reach the anterior

aspect of the distal articulation on metapodials. The intermediate relief is moderately high and quite sharp on the McIII, but low and smooth on medial and lateral metapodials.

McII. In proximal view, the proximal side consists of a large tear-shaped trapezoid-facet medial to a narrow sagittally-elongated and strip-like magnum-facet. In medial view, the trapezium-facet is large and comma shaped, higher in its posterior tip. In lateral view, the magnum-facet is a straight and low strip, separated from the McIII-facets over their length. The McIII-facets are fused into a curved strip with a shallow disto-median constriction. The distal articulation, for the phalanx 1, has a sub-square outline in distal view, with rounded anterior angles. It is overhung by a wide and salient medial tuberosity (Fig. 7, A).

McIII. The bone has a straight shaft. The proximal side is dominated by a wide and pentagonal magnum-facet, contiguous to two narrow sagittal strip-shaped facets (medially for the McII and laterally for the McIV). In anterior view, the proximal side consists of a subvertical medial edge (McII-facet), a very wide magnum-facet, weekly-concave medially, and a much narrower, oblique and straight McIV-facet. The magnum-facet is almost invisible in anterior view. Indeed, its dorsal outline is not much convex in medial view. The McII-facets are broadly connected, forming a thick strip with a shallow constriction in its disto-median part. In lateral view, the anterior McIV-facet is low, elongated sagittally, and tear-shaped. It is disconnected from the oval posterior McIV-facet by a narrow but deep oblique groove. This articulated surface overhangs a deep circular depression. There is no postero-distal tubercle on the diaphysis. In distal view, the distal articulation is wide and subrectangular, with straight medial and lateral edges, rounded antero-medial and -lateral angles, and a m-like posterior edge, due to a low but sharp intermediate relief (Fig. 7, B).

McIV. The McIV is the shortest and most robust metapodial preserved. The shaft is concave laterally in anterior view. The proximal aspect is trapezoid, deeper than wide, with a narrow medial strip (the sagittally-elongated ‘anterior’ McIII-facet) and a wide unciform-

facet. In proximal view, there is no postero-lateral pad, but a small anterolateral tubercle in front of the McV-facet. In medial view, the proximal McIII-facets are connected (right specimen) and determine the right dihedron (L-shape), with a high posterior facet. The McV-facet is vertical, suggesting a functional McV, in good agreement with the orientation of the McV-facet on the unciform. In distal view, the distal articulation forms a quarter circle, with a posteromedial right angle. There is almost no intermediate relief on the McIV (Fig. 7, C).

Phalanges. Only three phalanges are preserved for the manus (left/right first phalanges and left second phalanx for the McII). They have strong interphalangeal insertions and tubercles. The phalanx 1 is low and massive, with a kidney-like proximal side (McII-facet, lacking a groove responding to the intermediate relief). The distal facet is oval and transversely transversally elongated. The phalanx 2 is still lower, with a proximal facet perfectly matching in shape the distal facet on the phalanx 1. The distal facet is slightly concave transversally and convex sagittally. Both facets have similar width and depth.

Coxal. The pubic bones and ischia are lacking on both sides but the ilia are well preserved. Dorsally, the iliac crest is regularly convex. The wing of the ilium is spatulated. The sacral tuberosity has a rounded triangular shape, with a rugose aspect. The coxal tuberosity, partly broken, was probably thick and high, also with a rugose aspect. The caudal gluteal line is smooth, with a concave outline (forming a semi-circular curve). The acetabulum has a subcircular outline.

Femur. The bone is quite slender, with a shaft straight in anterior view, concave anteriorly in lateral view, and compressed sagittally (Fig. 8, A-F). The anterior part of the trochanter major is high, but the caudal part is very low, i.e., much lower than the wide and hemispheric head. The fovea capitis is deep, low, and wide, with a triangular outline. The lesser trochanter is elongated dorsoventrally. Its distal end reaches the mid-height of the third trochanter. The latter is developed, wider distally and with smooth lateral borders. The

anteroproximal border of the patellar condyle is curved, with a medial lip much more developed and salient than its lateral counterpart. In lateral view, the medial lip of the trochlea and the diaphysis determine a broken angle (130°). In distal view, the anterior border of the patellar trochlea is convex medially and straight and transverse laterally. The tibial condyles are separate from the patellar trochlea by a narrow groove. The intercondylar fossa is deep and narrow. The medial condyle, with a diamond-shaped outline, is much more developed than the lateral one. The medial epicondyle is also more salient than the lateral epicondyle.

Patella. The patella is massive, wider than high, and with a triangular and rugose anterior aspect. The medial border is straight and vertical. The posterior side, almost fully articulated, responds to the femoral cochlea, with a wide medial lip, triangular (wider distally), and a narrower trapezoid lateral lip. In vertical view, the latter lip is almost straight while the former is more concave. The most striking feature is the weak anteroposterior development of the bone.

Tibia. The tibia is high and relatively slender, with heavy extremities (Fig. 8, K-O). The medial border of the diaphysis is strikingly straight in anterior view, which widely contrasts with the concave lateral border of the shaft. This impression is highlighted by the median half of the proximal articulation being much higher than the lateral one. The proximal peroneal articulation is located low on the tibia (no contact with the lateral femoral condyle). There is neither an anterodistal groove nor medio-distal gutter (for the tendon m. tibialis posterior). Tibiae and fibulae are independent, apart from articulated areas, thus determining a wide *spatium interosseum cruris*. The distal fibula-facet is low, elongated, and crescent shaped, overhung by a rugose triangular area. The posterior apophysis is low and rounded. In distal view, the outline is a trapezoid, wider than deep. The astragalar cochlea has two lips, the medial one being narrower and deeper and the lateral one wider and shallower.

Fibula. The diaphysis is straight and particularly slender, in sharp contrast with two thick ends (and the robustness of the tibia) (Fig. 8, G-J). The proximal end is nevertheless flattened sagittally, with a smooth proximal tibia-facet. The distal end is robust, with a deep laterodistal gutter for the tendon m. peronaeus, located posteriorly, immediately posterior to a huge tubercle. The distal fibula-facet is low, elongated sagittally, and crescent shaped. It is contiguous to a flat and rectangular astragalus-facet, oriented at ~25° with respect to the vertical line.

The pes is not completely known. The naviculars, cuneiforms, MtIIIs, and most phalanges are not preserved. The metatarsals are shorter than the metacarpals.

Astragalus. The astragalus is thick (APD/H = 0.76), wide and low (TD/H = 1.29). The fibula-facet is subvertical, wide and flat dorsoventrally. The collum tali is very high (up to ¼ of the height), especially with respect to the general proportion of the bone. The caudal border of the trochlea is sinuous in dorsal view (with a falciform shape). There is no anterodistal trochlear notch, but a wide foramen for an insertion located distally to the concerned area, in the mid-collum tali. In anterior view, the distal border is deeply concave medially (navicular-facet) and straight and oblique laterally (cuboid-facet). The medial tubercle is low and rounded, but much projected medially. The distal articulation is not twisted with respect to the axis of the trochlea (<15°), in distal view. The calcaneus-facet 1 has a wide and very low, triangular laterodistal expansion. This facet is nearly flat in lateral view. The calcaneus-facets 2 (low oval) and 3 (tear shaped and low) are distinct and separate by a wide groove. In distal view, the distal articulation is much wider than deep, with a cuboid-facet particularly wide transversely. The posterior stop on that cuboid-facet is abrupt and prolongated medially by a similar transversely-elongated inflection on the navicular-facet.

Calcaneus. The calcaneus is robust, with a tuber calcanei massive and oval in posteroproximal view. This tuber calcanei is strongly vascularised and rugged with salient

muscle/tendon insertion areas, The tibia-facet is low, wide, and almond shaped, while the fibula-facet is round and oblique with respect to the vertical and sagittal lines. The astragalus-facet 1 is diamond shaped in anterior view and almost flat. The facet 2 is oval, wider than high and flat. It is separate from the smaller and semi-oval facet 3. The sustentaculum tali is low and very wide. In lateral view, the cuboid-facet and the posterior border of the tuber form a right angle and the processus is deeper (APD) than the tuber calcanei. The insertion for the m. fibularis longus forms a salient and rugose pad, but without sharp ridges. On the distal side, the cuboid-facet forms a transversely-elongated hexagon. It is flat except in its mediodistal quarter (concave).

Cuboid. The cuboid is compact, wide, and low. In proximal view, the large articular surface is oval, slightly tapering backwards, and split into two equally-developed and sagittally-elongated facets. The astragalus-facet (medial) is separated from the calcaneus-facet (lateral) by a narrow and shallow groove. The anterior side is low and pentagonal in anterior view, with a sharp proximal tip. In medial view, there are four facets. The anteroproximal one is very low and crescent like (navicular-facet). Distally to it is a much larger semi-circular ectocuneiform-facet. The posteroproximal navicular-facet, broadly joining the proximal facet for the astragalus, has an 8-shaped outline. Contiguous to it, but distally, is a semi-circular posterodistal ectocuneiform-facet. The posterior tuberosity is short sagittally and narrow, but quite elevated: its acuminated distal tip is way more distal than the distal articulation (MtIV-facet). The latter facet is flat and trapezoid, with larger anterior, medial, and posterior sides and a shorter lateral border. There is no MtIII-facet.

MtII. The bone is short and robust (Fig. 9, A). The proximal side, with a triangular outline (widening posteriorly), responds to the entocuneiform (posteromedial facet, pentagonal, and oblique), the mesocuneiform (proximal-most facet, wide and trapezoid), and to the ectocuneiform (wide strip-like facet oblique and tapering anteriorly). In lateral view, the

MtIII-facets are vertical, with a large triangular anterior facet and a much lower, oval posterior facet. Both are widely connected. The shaft is straight and subcircular in cross section. The distal end is stocky and square in distal view. The distal articulation has almost no intermediate relief, even in its posterior aspect.

MtIV. The bone is short and massive, with a heavy proximal end (Fig. 9, B). The proximal side is entirely occupied by a flat and sub-square cuboid-facet. There are two distinct proximal tubercles at the anterolateral and posterolateral angles, but no continuous pad. In medial view, there are two equally-wide MtIII-facets. The anterior one is located more dorsally, elevated and with a half-oval outline, connecting the proximal side. The posterior one is oval, isolated, and anteroventrally-posterodorsally elongated. The shaft is slightly concave laterally but straight in lateral view, with a strong laterodistal tubercle. The distal side is entirely articulated, deeper than wide (APD>TD), and lacking an intermediate relief. Only the lateral lip is slightly concave transversely in its posterior aspect.

Phalanges. Only the first phalanges for the MtII and MtIV are known. They have strong interphalangeal insertions and tubercles. There is no groove responding to the intermediate relief. The MtII phalanx 1 is almost cubic, with a circular and slightly biconcave proximal side (MtII-facet). The distal facet (phalanx 2) is kidney shaped. The MtIV phalanx 1 is as wide as but lower than the former phalanx. The proximal facet is kidney shaped and almost flat. The distal facet is oval and elongated transversely. In both phalanges, the distal facet is smaller than the proximal facet, but also slightly convex sagittally and concave transversely.

COMPARISON

The zygomatic arch is much narrower than in *Prosantorhinus* cf. *douvillei* from Béon 2, SW France (Antoine et al., 2018); the processus postorbitalis zygomaticus resembles that of *Brachydiceratherium* [*Bd.*] *aginense* (shape, absence of anterior inflection) (Fig. 10). Same

symphyseal region as in *Bd. aginense*. In *Bd. aginense*, there is a strong sexual dimorphism (I1s assignable to males are almost twice as large as those referable to females, with similar shape). The absence of p1/d1s is considered as a characteristic feature of *Bd. shanwangense.* No distal gutter is observable on the lateral epicondyle of the humerus, which makes it distinct from all representatives of *Brachydiceratherium*. The medial border of the glenoid fossa is straight, contrary to what is observed in *Bd. lemanense* and *Bd. aginense*. The carpus is lower and more massive than in *Bd. aginense*. The radius-ulna are more separate than in *Bd. aginense*.

The carpus and the metacarpus are comparable to those of the living white rhinoceros (*Ceratotherium simum*) in terms of proportions and robustness. In sharp contrast, the zeugopodium is much slenderer (*Dicerorhinus sumatrensis*-like; Guérin, 1980) whilst phalanges are much shorter.

On the femur, the femoral head is hemispherical and the caudal part of the trochanter major is very low, contrary to other representatives of *Brachydiceratherium*, except for *Bd. aginense* for the former feature and *P. douvillei* for the latter. The contrast between the lateral and medial lengths of the tibia is similar to what is observed in *Bd. aginense*. The insertions for the m. interossei are very long when compared to all teleoceratines.

PHYLOGENETIC ANALYSIS

A single most parsimonious tree is retrieved (length = 1315 steps; consistency index = 0.2700; retention index = 0.4923; Fig. 11; see S1 and S2). Twenty-four characters are constant, due to their original definition for solving phylogenetic relationships within Elasmotheriina (Antoine, 2002), a rhinocerotid subtribe the representatives of which are not included here. Character distribution at each node and corresponding indices are detailed in S2. Suprageneric relationships within Rhinocerotinae are consistent with those proposed by

Antoine (2002, 2003), Antoine et al. (2010, 2022), Becker et al. (2013), Tissier et al. (2021), and Pandolfi et al. (2021): *Plesiaceratherium mirallesi* is the earliest offshoot among Rhinocerotinae (node 1; 26 unambiguous synapomorphies; Bremer Support [BS] > 5). Aceratheriini (node 3; nine unambiguous synapomorphies; BS = 2) and Rhinocerotini (node 5; eight unambiguous synapomorphies; BS = 2) are sister clades (node 2; 13 unambiguous synapomorphies; BS = 4). Rhinocerotina (node 6; 18 unambiguous synapomorphies; BS > 5) and Teleoceratina (node 13; five dental and postcranial unambiguous synapomorphies; BS = 1) are sister clades within Rhinocerotini (Fig. 11). Aceratheriini comprise *Alicornops simorrense* as a sister species to the (*Aceratherium incisivum*, *Acerorhinus zernowi*) clade (node 4). Rhinocerotina include the (*Lartetotherium sansaniense*, *Gaindatherium browni*) clade (node 7; seven unambiguous synapomorphies; BS = 5) as the first offshoot, then *Nesorhinus philippinensis* (node 8; seven unambiguous synapomorphies; BS = 3), and the living rhino species (node 9; nine unambiguous synapomorphies; BS = 2), with the *Rhinoceros* clade (node 10; four unambiguous synapomorphies; BS = 1) being sister group to the (*Dicerorhinus sumatrensis* plus African rhinos) clade (node 11; 13 unambiguous synapomorphies; BS = 3). The clade of living African rhinos is the most supported node of the tree (node 12; 38 unambiguous synapomorphies; BS > 5).

In the next paragraphs, we will focus on the topology, node support (Bremer Support: BS), and apomorphy distribution regarding the Teleoceratina. The monophyly of the subtribe is weakly supported by five dental and postcranial unambiguous synapomorphies (BS = 1): I1 with an almond-shaped cross section, hypocone isolated by an anterior constriction on M2, ulna with the olecranon and the diaphysis forming a closed angle, robust limbs, and lateral metapodials with insertions of the m. interossei short. The earliest-diverging teleoceratine is *Diaceratherium tomerdingense*. This species is defined by ten dental and postcranial autapomorphies (teeth with enamel wrinkled and roots separate, P2-3 with an antecrochet

usually absent, M1-2 with a metaloph short, M2 with a mesostyle, humerus without a distal gutter on the lateral epicondyle, semilunate with a distal border of the anterior side rounded, trapezoid with a proximal border asymmetric in anterior view, unciform with a posterior expansion of the pyramidal-facet always present, and trapezium-facet always absent on the McII; Table 1). The next node (node 14) segregates the *Brachypotherium* clade (node 15) from all other teleoceratines scored here (node 16). The node 14 (BS = 2) is weakly supported by three postcranial unambiguous synapomorphies (proximal ulna-radius facets usually fused, gutter for the m. extensor carpi weakly developed on the radius, and McII with anterior and posterior McIII-facets fused). Eleven cranio-mandibular, dental, and postcranial synapomorphies define *Brachypotherium* (node 15; BS = 2): occipital condyle without a median ridge, mandibular symphysis very massive, labial cingulum usually present on upper premolars and always present on upper molars, lower cheek teeth with a flat ectolophid, lower molars with a lingual opening of the posterior valley U-shaped, p2 with a paraconid reduced, radius-ulna with a second distal articulation, pyramidal with a distal semilunate-facet asymmetric, posterior facet always absent on the McII-McIII, and fibula-facet oblique on the astragalus. The Bremer Support is low, due to an alternative topology with *B. perimense* being sister taxon to the (*B. brachypus*, node 16) clade appearing at 1317 steps. *Brachypotherium brachypus* are particularly well differentiated, with 27 unambiguous cranio-mandibular, dental, and postcranial autapomorphies each (see Table 1). From the node 16 diverge two clades, with (*Teleoceras* plus *Prosantorhinus*) on the one hand (node 17), and all species classically assigned to *Diaceratherium* except the type species (node 20). The node 16 (BS = 2) is supported by eight cranio-dental and postcranial unambiguous synapomorphies: vomer rounded, protocone constriction usually absent on P3-4, antecrochet always present on P4, lingual cingulum always present on lower premolars, pyramidal- and McV-facets always separate on the unciform, McIV with a trapezoid outline in proximal view, calcaneus-facets 2

and 3 always independent on the astragalus, and fibula-facet always present on the calcaneus. The node 17 (BS = 4) places the highly-divergent *Teleoceras fossiger* (39 cranio-mandibular dental, and postcranial unambiguous autapomorphies; Table 1) as sister species to *Prosantorhinus*, through 14 cranio-mandibular, dental, and postcranial synapomorphies: base of the processus zygomaticus maxillary low on the maxilla, zygomatic arch high, articular tubercle of the squamosal concave, lingual groove (sulcus mylohyoideus) absent on the corpus mandibulae, metaloph transverse and protoloph sometimes interrupted on P2, mesostyle present on M2, d2 with a posterior valley usually open, scapula spatulated and with a medial border straight on the glenoid fossa, a trochanter major low on the femur, MtII-facet always absent and cuboid-facet present on the MtIII, and metapodials with high and acute intermediate reliefs. *Prosantorhinus* (node 18; BS = 4) is monophyletic, with *P. germanicus* (thirteen cranio-dental unambiguous autapomorphies; Table 1) as the first offshoot (node 18) and *P. laubei* and *P. douvillei* being sister species (node 19). The monophyly of *Prosantorhinus* is supported by seven cranio-dental unambiguous synapomorphies, some being optimised in *P. laubei* (no cranial remains available; Heissig & Fejfar, 2007): lateral apophysis present on the nasals, median nasal horn present (probably in males), presence of a sagittal fronto-parietal crest, of a posterior groove on the processus zygomaticus of the squamosal, of a metacone fold on M1-2, of an unconstricted metaloph on M1, and of an ectolophid fold on d2-3. *Prosantorhinus douvillei* (nine unambiguous dental autapomorphies; Table 1) and *P. laubei* (six unambiguous dental autapomorphies; Table 1) share six dental and postcranial unambiguous synapomorphies (node 19; BS = 4): protocone unconstricted on P3-4 and M3, metaloph unconstricted on M2, labial cingulum always present on lower molars, lingual groove always present on d3, and expansion of the calcaneus-facet 1 always high and narrow on the astragalus.

The node 20 (BS = 3) gathers eight terminal taxa (Fig. 11). It is supported by ten cranio-dental and postcranial synapomorphies: nuchal tubercle small, articular tubercle smooth on the squamosal, cement present on cheek teeth, protocone always constricted on P3-4, labial cingulum usually absent on lower premolars and always present on lower molars, foramen vertebrale lateralis present and axis-facets transversally concave on the atlas, postero-distal apophysis low on the tibia, and latero-distal gutter located posteriorly on the fibula. Two clades diverge from the node 20. The first one (node 21, BS = 3) gathers *Brachydiceratherium shanwangense*, *Bd. aginense*, and *Bd. intermedium*, based on eight dental and postcranial synapomorphies: I1 with an oval occlusal outline, labial cingulum always absent on upper premolars, crista usually present on P3, scapula elongated, fossa olecrani high on the humerus, fovea capitis low and wide on the femur, latero-distal gutter deep on the fibula, limbs slender, and insertions for the m. interossei long on lateral metapodials. Most of them are optimised in *Bd. intermedium*. *Brachydiceratherium shanwangense* is well diagnosed, with sixteen cranio-dental and postcranial unambiguous synapomorphies: lateral apophysis present on the nasals, median nasal horn present on the nasals, premolar series short with respect to the molar series, roots distinct on the cheek teeth, crochet always simple and lingual cingulum usually absent and always reduced on P2-4, crista always present on P3, protocone strongly constricted on M1-2, lingual cingulum usually absent on lower premolars and always absent on lower molars, d1/p1 absent in adults, glenoid fossa with a medial border straight on the scapula, distal gutter absent on the lateral epicondyle of the humerus, proximal radius-ulna facets always fused, and trochanter major low on the femur. The node 22 (BS = 3) is supported by five dental and postcranial unambiguous synapomorphies: metaloph short on M1-2, posterior height exceeding the anterior height on the scaphoid, astragalus almost as high as wide (TD/H ratio between 1 and 1.2), and tibia- and fibula-facets absent on the calcaneus. *Brachydiceratherium intermedium*

(five dental and postcranial unambiguous autapomorphies; Table 1) is less differentiated than *Bd. aginense* (16 dental and postcranial unambiguous autapomorphies; Table 1), which probably reflects the strong contrast in the completeness of their hypodigms (e.g., no undisputable cranial remains are documented for *Bd. intermedium*).

The second clade diverging from the node 20 (i.e., node 23) places *Bd. fatehjangense* as a sister taxon to (*Bd. aurelianense*, (*Bd. lamilloquense*, (*Bd. lemanense*, *Bd. asphaltense*))). All the corresponding nodes are weakly supported (1 ≤ BS ≤3), with low numbers of unambiguous synapomorphies (ranging from three to six). The node 23 is the weakest one (BS = 1), with five dental and postcranial synapomorphies (metacone fold present on M1-2, second distal radius-ulna articulation present, posterior expansion of the scaphoid-facet low on the radius, postero-proximal semilunate-facet usually absent on the scaphoid, and expansion of the calcaneus-facet 1 usually wide and low on the astragalus.

DISCUSSION

Palaeobiological features

Both the complete dental eruption and the wear stages of upper and lower teeth concur to consider this individual as an adult, most likely ~7-15 years old (with reference to recent rhinos; e.g., Hillman-Smith et al., 1986; Hullot et al., 2020). In the absence of I1s (usually highly dimorphic in teleoceratines), and due to the fragmentary state of i2s, it is not possible to determine its sex.

Taxonomic inferences

Surprisingly, *Diaceratherium tomerdingense* Dietrich, 1931 is retrieved as the first offshoot among Teleoceratina (Fig. 11). Moreover, the assignment of this hornless and robust-limbed rhinocerotine to the subtribe is not well supported at all (BS = 1): in other words, this species could be closely related to Rhinocerotina instead among Rhinocerotini, as suggested

by some of its peculiar features, retrieved as autapomorphies in the current analysis (metaloph short on M1-2; distal gutter on the lateral epicondyle absent on the humerus, distal border of the anterior side of the semilunate rounded, and trapezium-facet absent on the McII). Accordingly, and given both the topology of the most parsimonious tree and the character distribution along its branches, we propose that *Diaceratherium* Dietrich, 1931 shall be restricted to the type species.

Indeed, all other species previously assigned to *Diaceratherium* in the last decades form a well-supported clade remote from the type species (Fig. 11). This clade is split into two sister clades encompassing three and five species, respectively (*D. shanwangense*, *D. aginense*, and *D. intermedium*; *D. fatehjangense*, *D. aurelianense*, *D. lamilloquense*, *D. asphaltense*, and *D. lemanense*). Except for *D. lamilloquense* Michel, 1987, these species were originally or subsequently assigned to pre-existing genera, i) either unambiguously non-related to Teleoceratina, such as *Aceratherium* (*D. lemanense*), *Diceratherium* (*D. asphaltense*, *D. lemanense*), *Aprotodon* (*D. fatehjangense*), *Chilotherium* or *Subchilotherium* (*D. intermedium*), and *Plesiaceratherium* (*D. shanwangense*), or ii) among Teleoceratina, with *Teleoceras* and/or *Brachypotherium* (*D. aginense*, *D. aurelianense*, *D. shanwangense*, and *D. fatehjangense*). Finally, and to our knowledge, the only species belonging to this clade for which a genus-group name has been unambiguously proposed is *D. lemanense*. Indeed, Lavocat (1951) has erected the subgenus *Brachydiceratherium* for "*Acerotherium lemanense* Pomel, 1853". Interestingly, Lavocat did assign these species and subgenus to *Diceratherium* Marsh, 1875, a genus consistently assigned to Elasmotheriinae in the last decades (e.g., Antoine, 2002). We propose that all these eight species be assigned to *Brachydiceratherium* Lavocat, 1951, especially as the five-species clade, with *D. fatehjangense*, *D. aurelianense*, *D. lamilloquense*, *D. asphaltense*, and *D. lemanense*, is not quite supported (BS = 1; 5 unambiguous synapomorphies). Noteworthily, *D. asphaltense* and *D. lemanense* are sister

species in the most parsimonious tree and given their low number of morpho-anatomical discrepancies, they could be considered as well as intraspecific variants within *D. lemanense* (senior synonym).

Other teleoceratine genera are monophyletic in the present analysis. *Brachypotherium* Roger, 1904 includes *B. brachypus* and *B. perimense* and this genus is a sister group to a clade gathering *Teleoceras* Hatcher, 1894 plus *Prosantorhinus* Heissig, 1974 on one branch and *Brachydiceratherium* on the other one (see above).

Historical biogeography of Eurasian teleoceratines

During early Miocene times, Teleoceratina were particularly species-rich in Eurasia, with 5–8 coeval species in any time slices (Fig. 12). A common thread between *Brachypotherium*, *Brachydiceratherium*, and *Prosantorhinus* is their huge geographical range at the generic level, encompassing most of the Eurasian landmasses for the latter two genera (e.g., Heissig, 1999; Antoine et al., 2010, 2013), plus Afro-Arabia for *Brachypotherium* (e.g., Hooijer, 1963, Geraads & Miller, 2013; Pandolfi & Rook, 2019). An early representative of *Brachydiceratherium* has been recognised in Thailand (*Bd*. cf. *lamilloquense*; Marivaux et al., 2004). It has the closest affinities with *Bd. lamilloquense*, from the late Oligocene of Western Europe (Fig. 13). To our knowledge, no occurrence has been reported between both areas for this species. *Prosantorhinus* has a similar geographical range, extending from Western Europe (*P. germanicus* and *P. douvillei*; Antoine et al., 2000; Heissig, 2017) and Central Europe (*P. laubei*; Heissig & Fejfar, 2007) to Southern Pakistan (*P. shahbazi*; Antoine et al., 2010, 2013). The recognition of *Bd. fatehjangense* in lower Miocene beds of the Turgai region in Kazakhstan, previously described as a representative of *Bd. aurelianense* by Borissiak (1927) and Lu et al. (2021), considerably expands latitudinally the range of this species, previously restricted to the Indian Subcontinent. It is now documented on both sides of the Himalayas (Fig. 13). The ubiquitous distributions of most teleoceratine taxa likely

underline ultra-generalist ecological preferences (Hullot et al., 2021). Moreover, such ranges seemingly support the absence of efficient ecological and geographical barriers at the Eurasian scale for the concerned teleoceratines, at least by early Miocene times (Fig. 13).

Moreover, ghost lineages within *Brachypotherium* and *Prosantorhinus* (Fig. 12) are likely to be bridged by *B. gajense* and *P. shahbazi*, from the latest Oligocene–earliest Miocene and the early Miocene of Pakistan, respectively (for further discussion, see Antoine et al., 2013 and Antoine, in press).

Brachydiceratherium shanwangense was previously only documented at Shanwang, eastern China (N32°, E116.5°). The well-supported specific assignment of the Tagay rhinoceros (N53°, E107.5°) points to an unsuspectedly wide geographical range for this species, further pleading for both a low climatic and environmental gradient in the concerned area at that time and very broad ecological preferences for this species (Fig. 13). Moreover, it can be suspected that the smallest teleoceratine remains described over the early Miocene interval in Japan (Kani and Mizunami formations) and referred to the *Brachypotherium pugnator* (Matsumoto, 1921), of gigantic dimensions (Fukuchi & Kawai, 2011; Tomida et al., 2013; Handa, 2020), may have particularly close affinities with those of *Bd. shanwangense*. More generally, the concerned Japanese assemblages are very similar to the Tagay and Shanwang ones, thus strengthening the existence of a single eastern Asian biogeographical province at mid latitudes at that time (Fig. 13). Indeed, closed forest environments under a subtropical climate, with precipitation averaging ca. 1500 mm per year, are reported for the Shanwang Basin based on early Miocene floras and vertebrates (Lu et al., 2021). The same proxies allow for considering the Tagay area as a lake, also surrounded by dense forests under subtropical conditions, with precipitation averaging ca. 1000-1500 mm per year (Logachev et al, 1964; Belova, 1985; Sizov & Klementiev, 2015).

CONCLUSIONS

The numerous associated features documented and scored in the Tagay rhinocerotid skeleton have allowed for assigning it to the same teleoceratine species (*Brachydiceratherium shanwangense*) as in Shanwang, eastern China. These remains further contribute to a refined depiction of phylogenetic relationships and to a revision of generic assignments among Eurasian Teleoceratina.

The genus *Diaceratherium* Dietrich, 1931 shall be restricted to the type species, *Diaceratherium tomerdingense* Dietrich, 1931. This monotypic genus is the first offshoot within Teleoceratina. Our results support the reappraisal of *Brachydiceratherium* Lavocat, 1951, with eight assigned species: *Brachydiceratherium lemanense* (Pomel, 1853), *Brachydiceratherium aurelianense* (Nouel, 1866), *Brachydiceratherium intermedium* (Lydekker, 1884), *Brachydiceratherium asphaltense* (Depéret & Douxami, 1902), *Brachydiceratherium fatehjangense* (Pilgrim, 1910), *Brachydiceratherium aginense* (Répelin, 1917), *Brachydiceratherium shanwangense* (Wang, 1965) and *Brachydiceratherium lamilloquense* Michel, 1983. *Brachydiceratherium* is a sister group to a clade encompassing *Prosantorhinus* and the North American genus *Teleoceras*. *Brachypotherium* is more closely related to the latter three genera than to *Diaceratherium*.

All Old World teleoceratines have extended geographical distributions at the genus level, which is also true for some species, such as the late Oligocene *Brachydiceratherium lamilloquense* and the early Miocene *Brachydiceratherium shanwangense*. The latter range supports the existence of a single eastern Asian biogeographical province at mid latitudes at that time for such megaherbivores.

ACKNOWLEDGMENTS

We are grateful to our colleagues for having participated in the 2008-2021 excavations. Special thanks to Gennady Turkin for logistical support and for assistance in the field. Valeria

Burova and Ekaterina Nikulina are acknowledged for working on the skeleton reconstruction. Muséum National d'Histoire Naturelle (Paris, France) kindly provided access to zoological and paleontological collections in their care and, personally, Christine Argot.

REFERENCES

Antoine P-O. 2002. Phylogénie et évolution des Elasmotheriina (Mammalia, Rhinocerotidae). *Mémoires du Muséum National d'Histoire Naturelle* **188**: 1–359.

Antoine P-O. in press. Rhinocerotids from the Siwalik faunal sequence. In: Badgley, C., Pilbeam, D. & Morgan, M. (Eds.), *At the Foot of the Himalayas: Paleontology and Ecosystem Dynamics of the Siwalik Record of Pakistan*. Johns Hopkins University Press.

Antoine P-O, Welcomme J-L. 2000. A new rhinoceros from the Bugti Hills, Baluchistan, Pakistan: the earliest elasmotheriine. *Palaeontology* **43**: 795–816.

Antoine P-O, Fleury G, Duranthon F. 2002. Le rhinocérotidé *Prosantorhinus douvillei* (Osborn, 1900) de l'Orléanien supérieur de Captieux (Gironde). *Bulletin de la Société d'Histoire Naturelle de Toulouse* **137**: 87–91.

Antoine P-O, Duranthon F, Welcomme J-L. 2003. *Alicornops* (Mammalia, Rhinocerotidae) dans le Miocène supérieur des Collines Bugti (Balouchistan, Pakistan): implications phylogénétiques. *Geodiversitas* **25**: 575–603.

Antoine P-O, Ducrocq S, Marivaux L, Chaimanee Y, Crochet J-Y, Jaeger J-J, Welcomme J-L. 2003. Early rhinocerotids (Mammalia: Perissodactyla) from South Asia and a review of the Holartic Paleogene rhinocerotid record. *Canadian Journal of Earth Sciences* **40**: 365–374.

Antoine P-O, Downing KF, Crochet J-Y, Duranthon F, Flynn LJ, Marivaux L, Métais G, Rajpar AR, Roohi G. 2010. A revision of *Aceratherium blanfordi* Lydekker, 1884

(Mammalia: Rhinocerotidae) from the Early Miocene of Pakistan: postcranials as a key. *Zoological Journal of the Linnean Society* **160**: 139–194.

Antoine P-O, Becker D. 2013. A brief review of Agenian rhinocerotids in Western Europe. *Swiss Journal of Geosciences* **106**: 135–146.

Antoine P-O, Becker D, Laurent Y, Duranthon F. 2018. The Early Miocene teleoceratine *Prosantorhinus* aff. *douvillei* (Mammalia, Perissodactyla, Rhinocerotidae) from Béon 2, Southwestern France. *Revue de Paléobiologie* **37**: 367–377.

Antoine P-O, Reyes MC, Amano N, Bautista AP, Chang CH, Claude J, Vos JD, Ingicco T. 2022. A new rhinoceros clade from the Pleistocene of Asia sheds light on mammal dispersals to the Philippines. *Zoological Journal of the Linnean Society* **194**: 416–430. DOI: 10.1093/zoolinnean/zlab009

Becker D, Antoine P-O, Maridet O. 2013. A new genus of Rhinocerotidae (Mammalia, Perissodactyla) from the Oligocene of Europe. *Journal of Systematic Palaeontolo*gy **11**: 947-972.

Belova VA. 1985. *Vegetation and climate of the Late Cenozoic of the south of Eastern Siberia*. Novosibirsk: Nauka [in Russian].

Boada-Saña A. 2008. *Phylogénie du rhinocérotidé* Diaceratherium Dietrich, 1931 *(Mammalia, Perissodactyla).* Master thesis dissertation. University of Montpellier, France, 2.

Boivin M, Marivaux L, Antoine P-O. 2019. L'apport du registre paléogène d'Amazonie sur la diversification initiale des Caviomorpha (Hystricognathi, Rodentia) : implications phylogénétiques, macroévolutives et paléobiogéographiques. *Geodiversitas* **41**: 143–245.

Borissiak A. 1914. On the dental apparatus of *Elasmotherium caucasicum* n. sp. *Bulletin de l'Académie Impériale des Sciences de St-Pétersbourg* **6**: 555–584.

Borissiak A. 1927. *Brachypotherium aurelianense* Nouel, var. nov. Gailiti, from the Miocene deposits of the Turgai region. *Bulletin de l'Académie des Sciences de l'URSS* **21**: 273–286.

Burchell WJ. 1817. Note sur une nouvelle espéce de Rhinoceros. *Bulletin de la Société Philomathique de Paris (June)*.

Cerdeño E. 1993. Étude sur *Diaceratherium aurelianense* et *Brachypotherium brachypus* (Rhinocerotidae, Mammalia) du Miocène moyen de France. *Bulletin du Muséum national d'Histoire naturelle* **15**: 25–77.

Cerdeño E. 1995. Cladistic analysis of the Family Rhinocerotidae (Perissodactyla). *American Museum Novitates* **3143**: 1–25.

Crusafont M, Villalta JF, Truyols J. 1955. El Burdigaliense continental de la Cuenca del Vallés-Penedés. *Memorias y Comunicaciones del Instituto Geológico, Barcelona* **12**: 1–272.

Danilov IG, Syromyatnikova EV, Klementiev AM, Sizov AV, Martynovich NV, Zelenkov NV, Sychevskaya EK, Tesakov AS. 2012. New data on Miocene vertebrates of Tagay locality (Olkhon, Lake Baikal). In: Lopatin AV, Parkhaev PYu, Rozanov AYu eds. *Modern Paleontology: classical and new methods. The ninth all-Russian scientific school for young scientists in Paleontology.* Moscow: Paleontological Institute 19–20 [in Russian].

Daxner-Höck G, Böhme M, Kossler A. 2013. New Data on Miocene Biostratigraphy and Paleoclimatology of Olkhon Island (Lake Baikal, Siberia). In: Wang X, Flynn LJ, Fortelius M, eds., *Fossil mammals of Asia: Neogene biostratigraphy and chronology*, New York: Columbia University Press, 508-517.

Depéret C, Douxami H. 1902. Les Vertébrés oligocènes de Pyrimont-Challonges (Savoie). *Mémoires suisses de Paléontologie* **29**: 1–92.

Dietrich WO. 1931. Neue Nashornreste aus Schwaben (*Diaceratherium tomerdingensis* n. g. n. sp.). *Zeitschrift für Säugetierkunde* **6**: 201–223.

Falconer H, Cautley PT. 1847. *Fauna antiqua Sivalensis, being the fossil zoology of the Sewalik Hills, in the North of India (Sus, Rhinoceros, Chalicotherium).* London: Smith, Elder and Co..

Filippov AG, Sytchevskaya EK. 2000. Remains of snakeheaded fishes (Channidae) near Lake Baikal. *The Third Vereshchagin Baikal Conference, Aug 22-27, Irkutsk*, 251.

Fischer von Waldheim GF. 1814. *Zoögnosia tabulis synopticis illustrate, in usum Paeselectionum Academiae Imperialis Medicochirurgae*. Moscow: Nicolai Sergeidis Vsevolozsky.

Fukuchi A, Kawai K. 2011. Revision of fossil rhinoceroses from the Miocene Mizunami Group, Japan. *Palaeontological Research* **15**: 247–257.

Geraads D, Miller E. 2013. *Brachypotherium minor* n. sp., and other Rhinocerotidae from the Early Miocene of Buluk. Northern Kenya. *Geodiversitas* **35**: 359–375. DOI: 10.5252/g2013n2a5.

Guérin C. 1980. Les rhinocéros (Mammalia, Perissodactyla) du Miocène terminal au Pléistocène supérieur en Europe occidentale. Comparaison avec les espèces actuelles. *Documents des Laboratoires de Géologie de Lyon* **79**: 1–1185.

Handa N. 2020. Reappraisal of a rhinocerotid (Mammalia, Perissodactyla) from the lower Miocene Yotsuyaku Formation, Northeast Japan, with an overview of the early Miocene Japanese rhinocerotids. *Paleontological Research* **24**: 183–191.

Heissig K. 1969. Die Rhinocerotidae (Mammalia) aus der oberoligozänen Spaltenfüllung von Gaimersheim bei Ingolstadt in Bayern und ihre phylogenetische Stellung. *Verlag der Bayerischen Akademie der Wissenschaften* **138**: 1–133.

Heissig K. 1972. Paläontologische und geologische Untersuchungen im Tertiär von Pakistan. 5 – Rhinocerotidae (Mamm.) aus den unteren und mittleren Siwalik-schichten. *Abhandlungen der Bayerischen Akademie der Wissenschaften, München, mathematische-naturwissenschaftliche Klasse* **152**: 1–112.

Heissig K. 1972. Die obermiozäne Fossil-Lagerstätte Sandelzhausen. 5. Rhinocerotidae (Mammalia), Systematik und Ökologie. *Mitteilungen der Bayerischen Staatssammlung für Paläontologie und historische Geologie* **12**: 57–81.

Heissig K. 1999. Family Rhinocerotidae. In: Röessner GE, Heissig K. eds. *The Miocene Land Mammals of Europe*. Dr Pfeil, Munich 175–188.

Heissig K, Fejfar O. 2007. Die fossilen Nashörner (Mammalia, Rhinocerotidae) aus dem Untermiozän von Tuchořice in Nordwestboehmen. *Acta Musei Nationalis Pragae B* **63**: 19-64.

Heissig K. 2012. Les Rhinocerotidae (Perissodactyla) de Sansan. *Mémoires du Muséum national d'Histoire naturelle de Paris* **203**: 317–485.

Heissig K. 2017. Revision of the European species of *Prosantorhinus* Heissig, 1974 (Mammalia, Perissodactyla, Rhinocerotidae). *Fossil Imprint* **122**: 265–294. DOI : 10.1515/if-2017-0014.

Hilgen FJ, Lourense LJ, Van Dam JA. 2012. The Neogene period. In: Gradstein FM, Ogg JG, Schmitz MD, Ogg GM, eds. *The Geologic Time Scale 2012*. Oxford: Elsevier 923–978.

Hooijer DA. 1963. Miocene Mammalia of the Congo. *Musée royal de l'Afrique Centrale. Annales - sciences géologiques* **46**: 1–77.

Hullot M, Laurent Y, Merceron G, Antoine P-O. 2021. Paleoecology of the Rhinocerotidae (Mammalia, Perissodactyla) from Béon 1, Montréal-du-Gers (late early

Miocene, SW France): Insights from dental microwear texture analysis, mesowear, and enamel hypoplasia. *Palaeontologia Electronica* **24**: a27. DOI: 10.26879/1163

Kitainik AF, Ivaniev LN. 1958. A note on the Tertiary deposits of Olkhon Island on Lake Baikal. *Notes of the Irkutsk Regional Museum of Local History* 55–60.

Klementiev AM. 2009. Finding a Miocene rhinoceros on Olkhon Island (Lake Baikal). In: Barskov IS & Nazarova VM eds. *200 years of national paleontology. Materials of the All-Russian meeting*. Moscow: Paleontological Institute, 56–57 [in Russian].

Klementiev AM, Sizov AV. 2015. New record of anchithere (*Anchitherium aurelianense*) in the Miocene of Eastern Siberia, Russia. *Russian Journal of Theriology* **14**: 133-143.

Kossler A. 2003. Neogene sediments of Olkhon and Svyatoy Nos (Baikal Rift System, East Siberia): Suggestions about the development of Lake Baikal. *Berliner Paläobiologische Abhandlungen* **4**: 55–63.

Khan MA, Akhtar M, Khan AM, Ghaffar A, Iqbal M, Samiullah K. 2011. New fossil locality in the Middle Miocene of Lava from the Chinji Formation of the Lower Siwaliks, Pakistan. *Pakistan Journal of Zoology* **43**: 61–72

Khosatzky LI, Chkhikvadze VM. 1993. New data about Miocene turtles of the genus *Baicalemys*. *Bulletin of the Academy of Science of Georgia* **148**: 155–160 [in Russian].

von Koenigswald GHR. 1956. Fossil Mammals from the Philippines. *National Research Council of the Philippines, University of the Philippines Diliman. Special reprint. Full text illustrations of paper 22 Proceedings of the Fourth Far-Eastern Prehistory Congress*: 1–14.

Kordikova EG. 2001. Remarks on the Oligocene-Miocene mammal paleontology and sequence stratigraphy of South-Western Betpakdala Steppe, South Kazakhstan. *Neues Jahrbuch für Geologie und Paläontologie Abhandlungen* **221**: 35–79.

Lartet E. 1851. *Notice sur la colline de Sansan*. Auch: Portes.

Laurillard F. 1848. Rhinocéros fossiles, in d'Orbigny CD (ed.), *Dictionnaire universel d'Histoire naturelle*, volume 11. Renard, Martinet & Cie, Paris: 99–102.

Linnaeus C. 1758. *Systema Naturae per regna tria naturae, secundum classes, ordines, genera, species, cum characteribus, differentiis, synonymis, locis.* Vol. 1. Tenth Edition. Stockholm: Regnum animale.

Logachev NA, Lomonosova TK, Klimanova VM. 1964. *The Cenozoic deposits of the Irkutsk amphitheatre*. Moscow: Nauka [in Russian].

Lavocat R. 1951. *Révision de la faune des mammifères oligocènes d'Auvergne et du Velay*. Sciences et Avenir, Paris.

Lu X, Cerdeño E, Zheng X, Wang S, Deng T. 2021. The first Asian skeleton of *Diaceratherium* from the early Miocene Shanwang Basin (Shandong, China), and implications for its migration route. *Journal of Asian Earth Sciences: X* **6**: 100074

Lydekker R. 1884. Additional Siwalik Perissodactyla and Proboscidea. *Memoirs of the Geologcal Survey of India – Palaeontologia Indica* **3**: 1–34.

MacFadden BJ. 1998. Equidae, In: Janis CM, Scott KM, Louis LL eds. *Evolution of Tertiary Mammals North America*. vol. 1. Cambridge University Press 537–559.

Marivaux L, Chaimanee Y, Yamee C, Srisuk P, Jaeger J-J. 2004. Discovery of *Fallomus ladakhensis* Nanda & Sahni, 1998 (Mammalia, Rodentia, Diatomyidae) in the lignites of Nong Ya Plong (Phetchaburi Province, Thailand): systematic, biochronological and paleoenvironmental implications. *Geodiversitas*, **26**: 493-507.

Mats VD, Ufimtsev GF, Mandelbaum MM., Alakshin AM, Pospeev AV, Shimaraev MN, Khlystov OM. 2001. *Cenozoic of the Baikal rift zone*. Novosibirsk: GEO SO RAS Press [in Russian].

Mats VD, Lomonosova TK, Vorobyeva GA, Vologina EG. 2010. Late Cretaceous-Cenozoic sediments of the Baikal rift basin and changing natural conditions. *Geodynamics & Tectonophysics* **1**: 75–86 [in Russian].

Mats VD, Yefimova IM. 2011. Paleogeographic scenario of the Late Cretaceous – Cenozoic for the central part of the Baikal region. *Geodynamics & Tectonophysics* **2**: 175–193 [in Russian].

Mats VD. 2013. Late Cretaceous and Cenozoic Stratigraphy of the Baikal Rift Sediments. *Stratigraphy and Geological Correlation* **21**: 637–651. DOI: 10.1134/S0869593813060075

Mats VD. 2015. The Baikal rift: Pliocene (Miocene) – Quaternary episode or product of extended development since the Late Cretaceous under various tectonic factors. A review. *Geodynamics & Tectonophysics* **6**: 467–489 [in Russian]. DOI: 10.5800/GT-2015-6-4-0190

Matsumoto H. 1921. Descriptions of some new fossil mammals from Kani District, Province of Mino, with revisions of some Asiatic fossil rhinocerotids. *The Science Reports of the Tohoku Imperial University. Second Series (Geology)* **5**: 75–91.

Ménouret B, Guérin C. 2009. *Diaceratherium massiliae* nov. sp. from the Oligocene clays of Saint-André and Saint-Henri in Marseille and Les Milles near Aix-en-Provence (South Eastern France), the first European large brachypod Rhinocerotidae. *Geobios* **42**: 293–327.

Nouel E. 1866. Mémoire sur un nouveau rhinocéros fossile. Mémoires de la Société d'Agriculture, Sciences, *Belle-Lettres et Art d'Orléans* **8**: 241–251.

Orliac MJ, Antoine P-O, Ducrocq S. 2010. Phylogenetic relationships of the Suidae (Mammalia, Cetartiodactyla): new insights on the relations within Suoidea. *Zoologica Scripta* **39**: 315–330.

Osborn HF. 1900. Phylogeny of the rhinoceroses of Europe. *Memoirs of the American Museum of Natural History* **13**: 229–267.

Pandolfi L, Rook L. 2019. The latest Miocene Rhinocerotidae from Sahabi (Libya). *Comptes Rendus Palevol* **18**: 442-448. DOI: 10.1016/j.crpv.2019.03.002.

Pandolfi L, Antoine P-O, Bukhsianidze M, Lordkipanidze D, Rook L. 2021. Northern Eurasian rhinocerotines (Mammalia, Perissodactyla) by the Pliocene–Pleistocene transition: phylogeny and historical biogeography. *Journal of Systematic Palaeontology.* DOI: 10.1080/14772019.2021.1995907

Pilgrim GE. 1910. Notice on new mammal genera and species from the Tertiaries of India. *Records of the Geological Survey of India* **15**: 63–71.

Pokatilov AG. 2004. *Paleontology and stratigraphy of the Cenozoic of the south of Eastern Siberia and adjacent territories*. Irkutsk: Irkutsk State Technical University Press [in Russian].

Pomel M. 1853. *Catalogue méthodologique et descriptif des vertébrés fossiles découverts dans le bassin hydrographique supérieur de la Loire, et surtout dans la vallée de son affluent principal, l'Allier.* Paris: Baillière Ed.

Prieto J., Antoine P-O, Böhme M, van der Made J, Métais G, Laq The Phuc, Quý Trương Quan, Schneider S, Dang Ngoc Tran, Vasilyan D, Luong The Viet, 2018. Biochronological and paleobiogeographical significance of the earliest Miocene mammal fauna from Northern Vietnam. *Palaeobiodiversity and Palaeoenvironments* **98**: 287–313. doi 10.1007/s12549-017-0295-y

Prothero DR, Guérin C, Manning E. 1989. The History of the Rhinocerotoidea. In: Prothero DR & Schoch RM eds. *The Evolution of Perissodactyls*, New York: Oxford University Press, 322–340.

Prothero DR. 2005. *The evolution of North American Rhinoceroses*. Cambridge; New York; Melbourne: Cambridge University Press.

Raffi I, Wade BS, Pälike H, Beu AG, Cooper R, Crundwell MP, Krijgsman W, Moore T, Raine I, Sardella R, Vernyhorova YV. 2020. Chapter 29 - The Neogene Period. In: Gradstein FM, Ogg JG, Schmitz MD, Ogg GM ads. *Geologic Time Scale 2020*. Elsevier 1141–1215. DOI: /10.1016/B978-0-12-824360-2.00029-2.

Rage JC, Danilov IG. 2008. A new Miocene fauna of snakes from eastern Siberia, Russia.: Was the snake fauna largely homogenous in Eurasia during the Miocene? *Comptes Rendus Palevol* **7**: 383–390. DOI: 10.1016/j.crpv.2008.05.004.

Répelin J. 1917. Études paléontologiques dans le sud-ouest de la France (Mammifères). Les rhinocérotidés de l'Aquitanien supérieur de l'Agenais (Laugnac). *Annales du Muséum d'Histoire naturelle de Marseille* **16**: 1–47.

Rössner G.E., Mörs T. 2001. A New Record of the Enigmatic Eurasian Miocene Ruminant Artiodactyl *Orygotherium*. *Journal of Vertebrate Paleontology* **21**: 591-595.

Sizov AV, Klementiev AM. 2015. Geology and taphonomy of Tagay locality of early Miocene vertebrate fauna. In: Lipnina EA & Berdnikov IM, eds. *Eurasia in the Cenozoic. Stratigraphy, paleoecology, cultures.* Irkutsk: Irkutsk State University Press, 206–218 [in Russian].

Sotnikova MV, Klementiev AM, Sizov AV, Tesakov AS. 2021. New species of *Ballusia* Ginsburg and Morales, 1998 (Ursidae, Carnivora) from Miocene of Eastern Siberia, Russia. *Historical Biology* **33**: 486-497, DOI: 10.1080/08912963.2019.1637864

Swofford, D.L. 2002. *PAUP*: Phylogenetic analysis using parsimony (*and other methods). Version 4.0b10*, Sunderland, Sinauer Associates, Inc., Publishers, Sunderland.

Syromyatnikova EV. 2014. The first record of *Salamandrella* (Caudata: Hynobiidae) from the Neogene of Russia. *Russian Journal of Herpetology* **21**: 217–220.

Syromyatnikova EV. 2015. A New Species of *Bufo* (Amphibia, Anura) from the Miocene of Russia. *Russian Journal of Herpetology* **22**: 281–288.

Tesakov AS, Lopatin AS. 2015. First record of Mylagaulid rodents (Rodentia, Mammalia) from the Miocene of Eastern Siberia (Olkhon Island, Baikal Lake, Irkutsk Region, Russia). *Doklady Biological Sciences* **460**: 23–26.

Tissier J, Antoine P-O, Becker D. 2021. New species, revision, and phylogeny of *Ronzotherium* Aymard, 1854 (Perissodactyla, Rhinocerotidae). *European Journal of Taxonom*y **753**: 1–80. DOI: 10.5852/ejt.2021.753.1389

Tissier J, Geiger-Schütz P, Flückiger PF, Becker D. 2021. Neue Erkenntnisse über die Nashorn-Funde von Rickenbach (SO) (Oberes Oligozän, Kanton Solthurn, Schweiz) aus der Sammlung des Naturmuseums Olten. *Naturforschende Gesellschaft des Kantons Solothurn* **44**: 25–50

Tomida Y, Nakaya H, Saegusa H, Miyata K, Fukuchi A. 2013. Miocene Land Mammals and Stratigraphy of Japan. In: Wang X, Flynn LJ, Fortelius M, eds., *Fossil mammals of Asia: Neogene biostratigraphy and chronology*, New York: Columbia University Press, 314–333.

Vislobokova IA. 1990. About artiodactyls from the Lower Miocene of the Tagay bay, Olkhon island (Baikal). *Paleontological Journal* **2**: 134–138 [in Russian].

Vislobokova IA. 1994. The Lower Miocene artiodactyls of Tagay Bay, Olkhon Island, Lake Baikal (Russia). *Palaeovertebrata*. **23**: 177–197.

Vislobokova I. 2004. New species of *Orygotherium* (Palaeomerycidae, Ruminantia) from the Early and Late Miocene of Eurasia. *Annalen des Naturhistorischen Museums in Wien* **106**: 371–385.

Wang KM. 1929. Die obermiozänen Rhinocerotiden von Bayern. *Paläontologische Zeitschrift*, **10**: 184-212.

Wang BY. 1965. A new Miocene aceratheriine rhinoceros of Shanwang, Shandong. *Vertebrata PalAsiatica* **9**: 109–112.

Zelenkov NV. 2016. The first fossil parrot (Aves, Psittaciformes) from Siberia and its implications for the historical biogeography of Psittaciformes. *Biology Letters* **12**: 20160717. DOI: 10.1098/rsbl.2016.0717

SUPPORTING INFORMATION

Additional supporting information may be found online in the supporting information tab for this article. Supplementary Files:

- **S1**. Character matrix for the phylogenetic analysis, including 282 cranial, dental, and postcranial characters controlled on 31 terminal taxa (one tapirid, rhinocerotoids, and rhinocerotids).
- **S2.** Buffer of the phylogenetic analysis, with Bremer Support
- **S3** Measurements for *Brachydiceratherium shanwangense* from Tagay site.

FIGURES

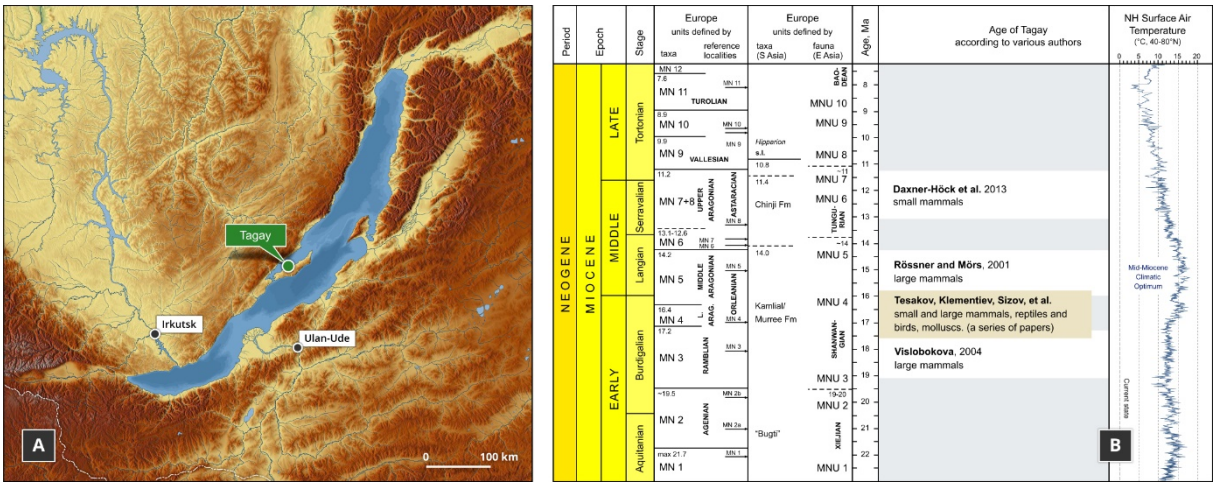

Fig. 1. Geographic position of Tagay locality (A) and age of Tagay Formation according to various authors (B). [Full width suggested]

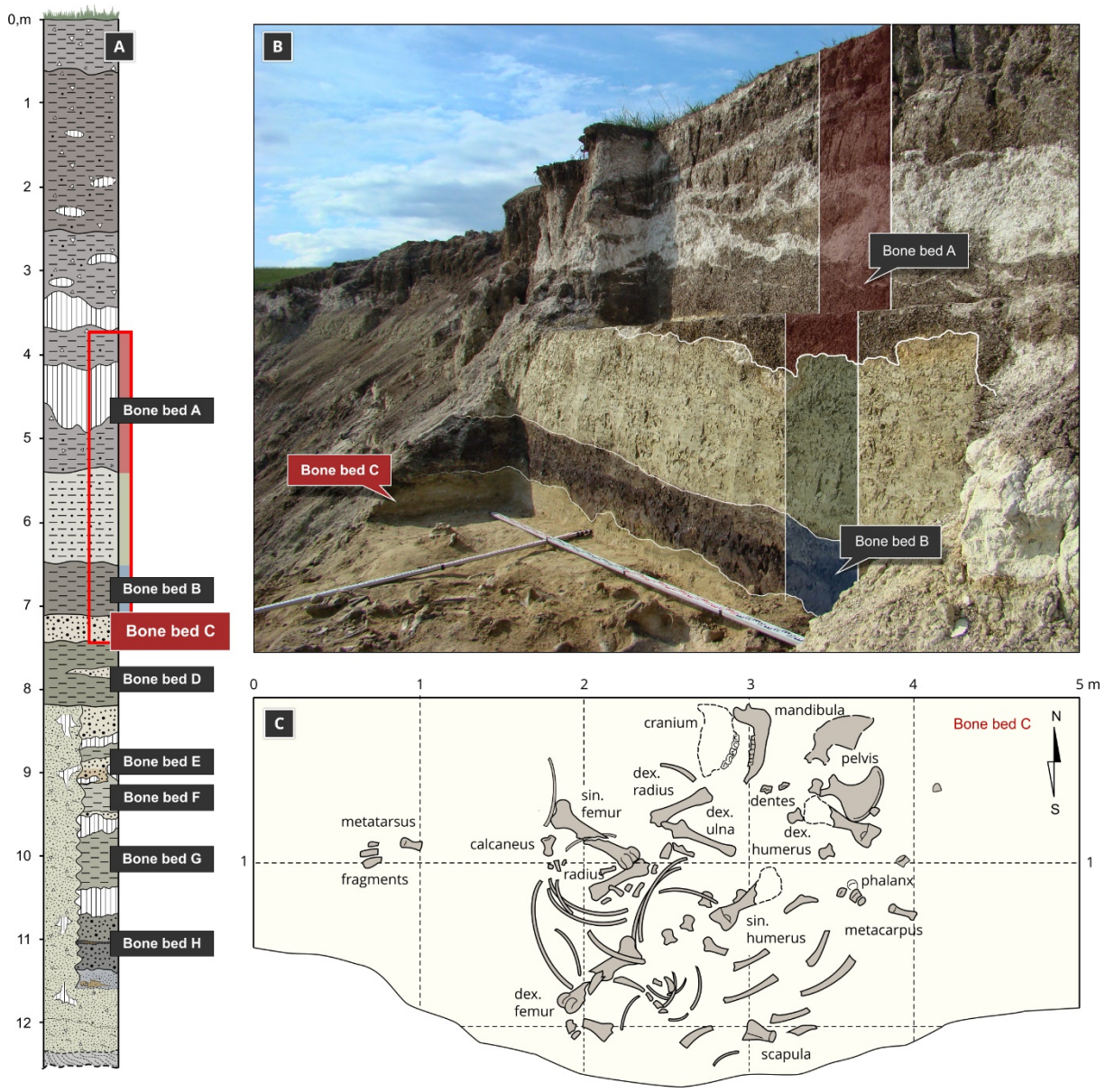

Fig. 2. Geological structure of the Tagay section (A), photo (B) and plan (C) of the excavations of the Miocene rhinocerotid at Tagay site in 2008. [Full width suggested]

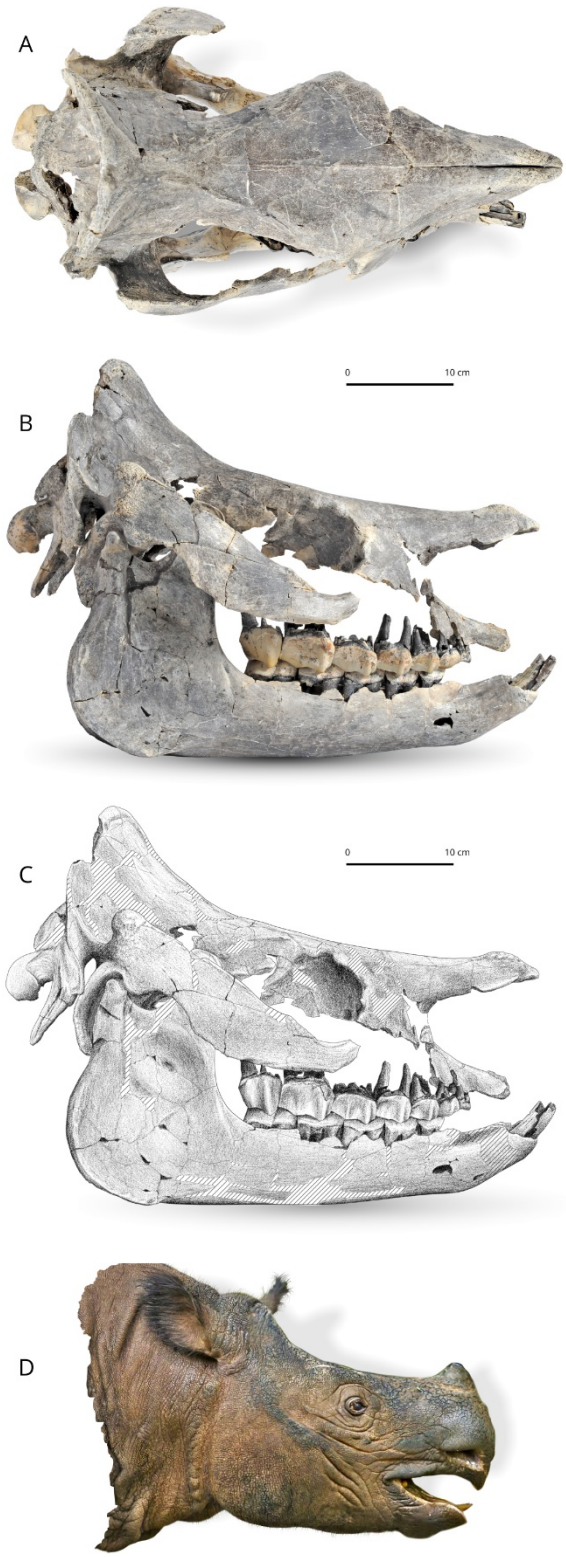

Fig. 3. *Brachydiceratherium shanwangense* (Wang, 1965). Photo (A) and scientific drawing (B) of the skull, based on skull and mandible IZK79-1-08C-1. Striped areas are reconstructed. C - reconstruction of the head based on the skull. [One column width suggested]

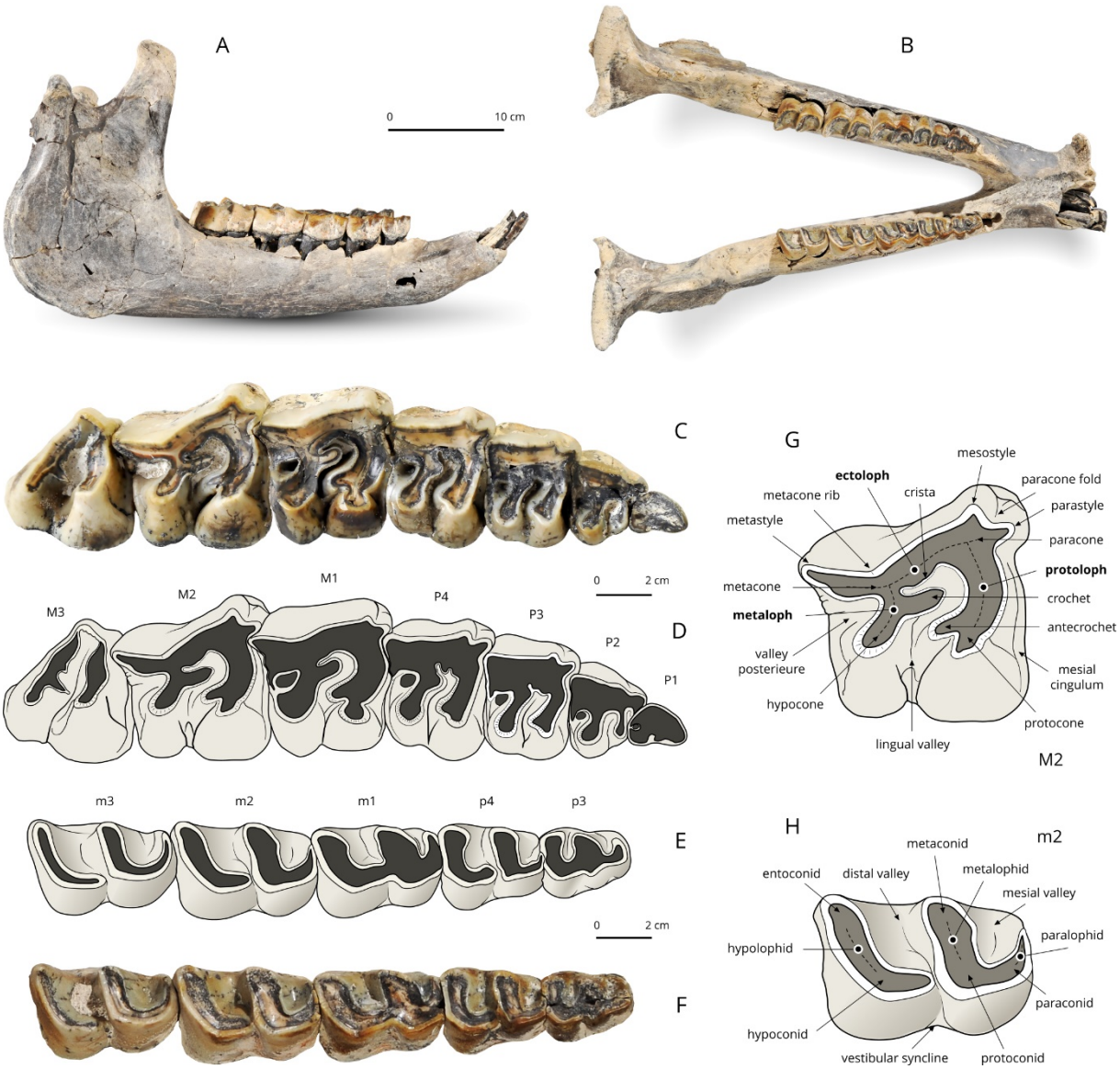

Fig. 4. The mandible and dental material. A, B – The mandible; C, D – Right upper cheek teeth (P3–M3); Right lower cheek teeth (p3–m3). Dental terminology for rhinocerotid upper tooth (G) and lower tooth (H). [Full width suggested]

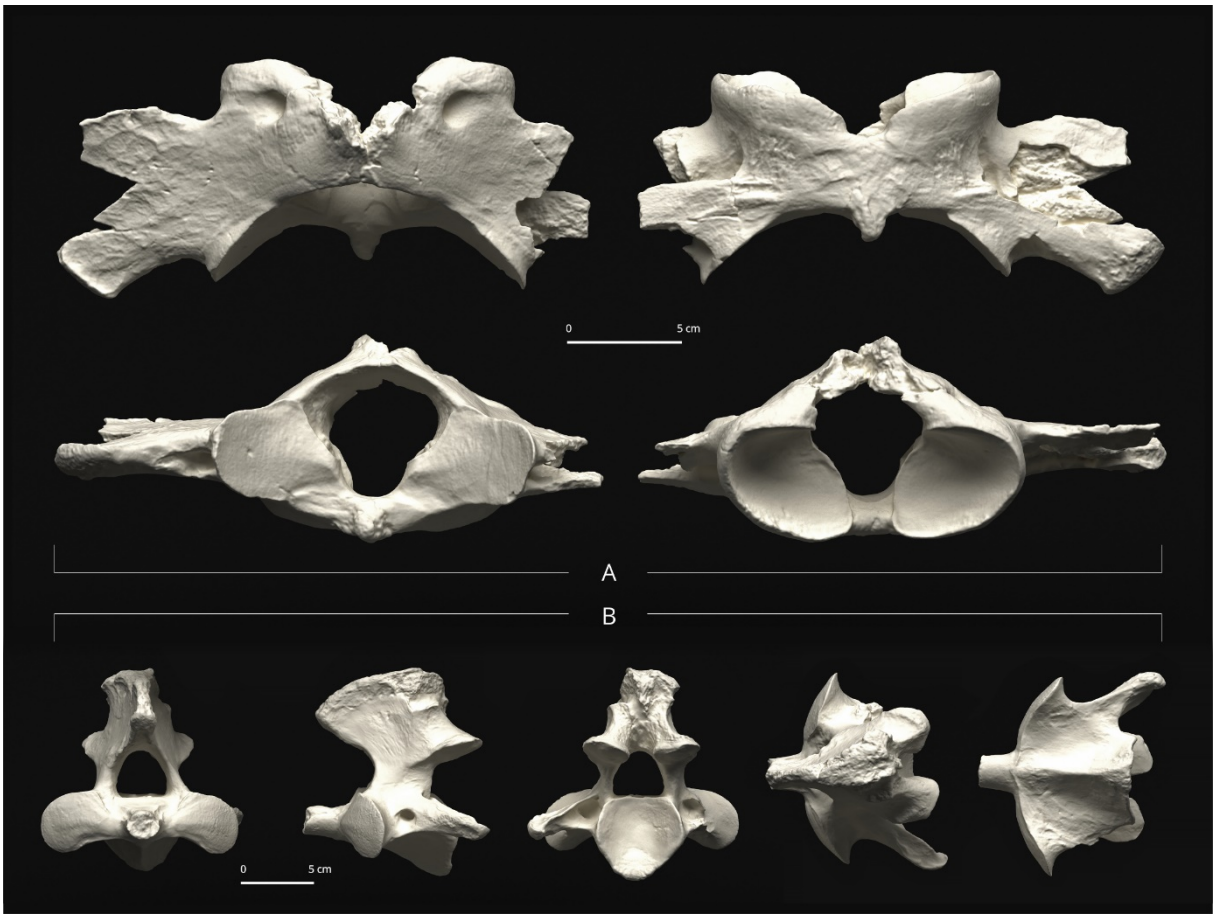

Fig. 5. Atlas (A) and Axis (B). [Full width suggested]

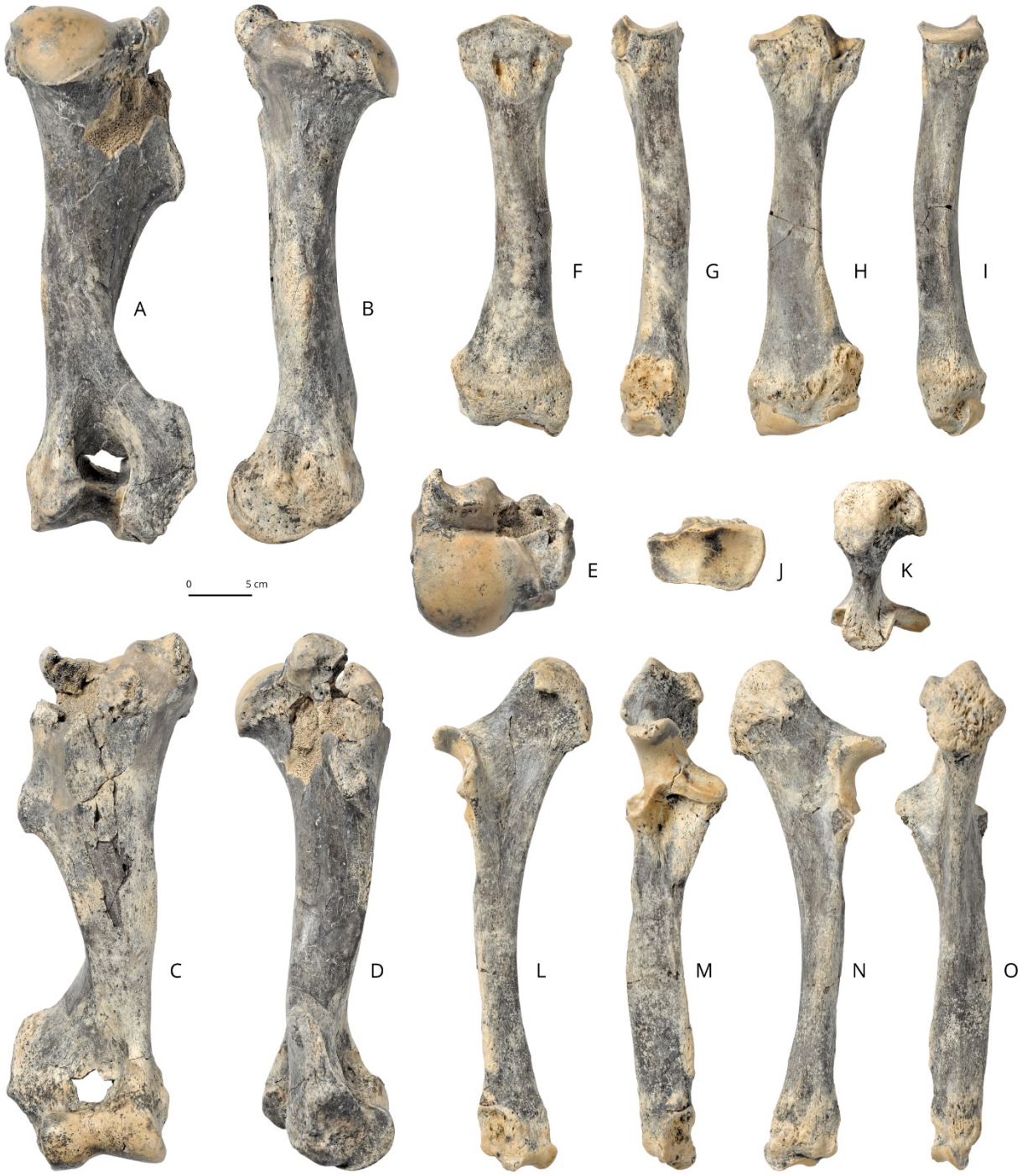

Fig. 6. Long bones of the right forelimb. A-E – humerus; F-J – radius; K-O – ulna. [Full width suggested]

Fig. 7. Left metacarpal bones. A – second metacarpal; B – third metacarpal; C – fourth metacarpal. [Full width suggested]

Fig. 8. Long bones of the left hind limb. A-F – femur; G-J – fibula; K-O – tibia. [Full width suggested]

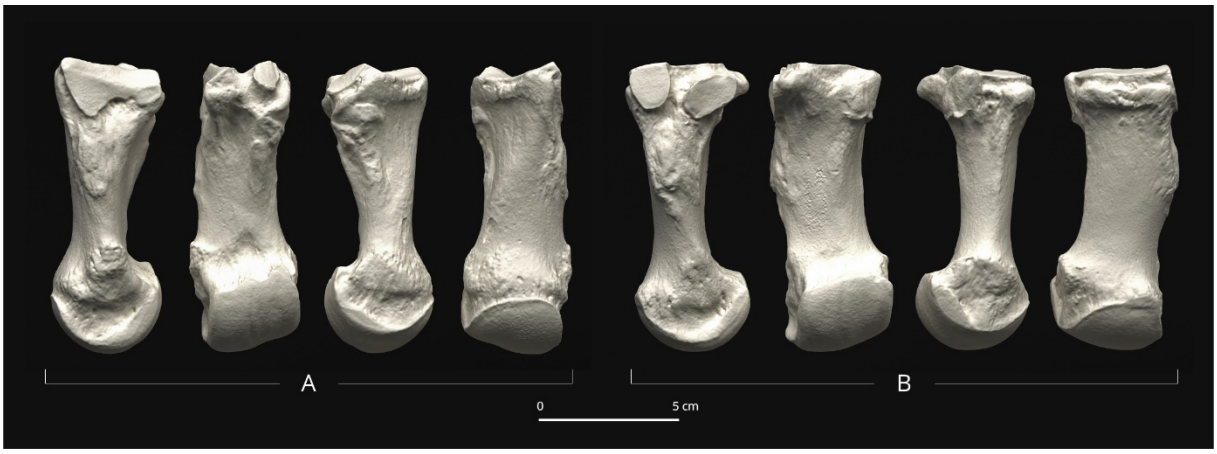

Fig. 9. Metatarsal bones. A – left second metatarsal; B – right fourth metatarsal. [Full width suggested]

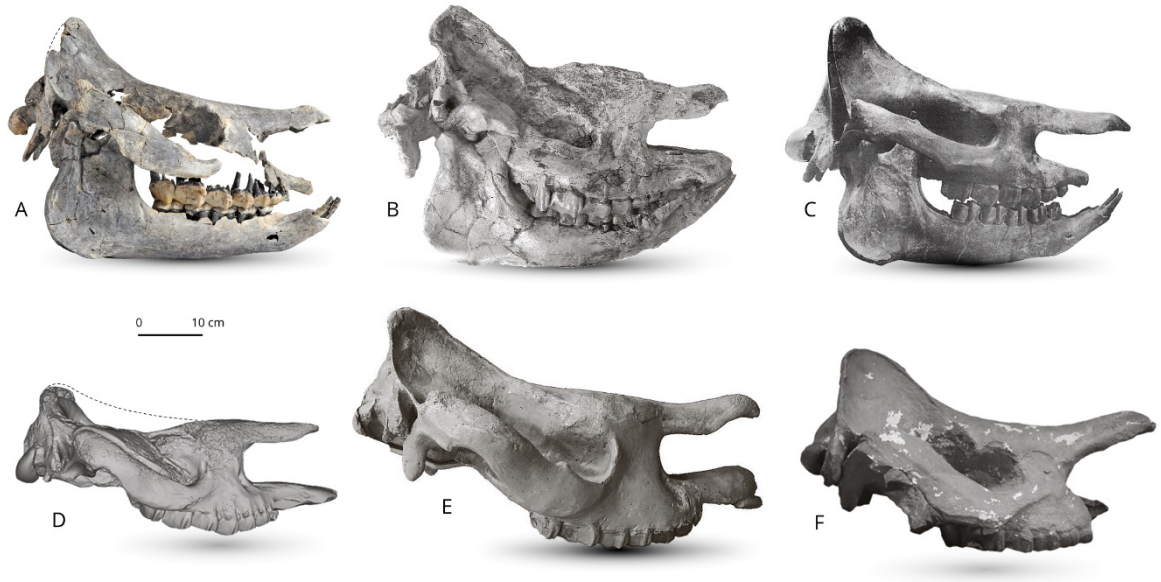

Fig. 10. Skulls of different species of *Brachydiceratherium* in lateral view. **A -** *Brachydiceratherium shanwangense* from Tagay (MN3-MN5? - Early Miocene, Baikal Region, Russia) №IZK79-1-08C-1/1; **B** - *Brachydiceratherium shanwangense* from Jijiazhuang locality STM 44–98 (deformed, mirrored) (MN4 - Early Miocene, Shanwang Basin, Shandong Province, China) №MHNT.PAL.2013.0.1001; **C** - *Brachydiceratherium aginense* (Répelin, 1917) from Laugnac (MN2 - Early Miocene, Lot-et-Garonne, France); **D** - *Brachydiceratherium lemanense* from Gannat (MN1 - Early Miocene, France) №MNHN-AC-2375, holotype; **E** - *Brachydiceratherium asphaltense* (Depéret et Douxami, 1902) from Saulcet (MN1 - Early Miocene, Allier, France). №NMB–Sau1662; **F** - *Brachydiceratherium aurelianense* from Neuville-aux-Bois (MN3 - Early Miocene, France) №MHNT.PAL.2013.0.1001, cast of the holotype; [Full width suggested]

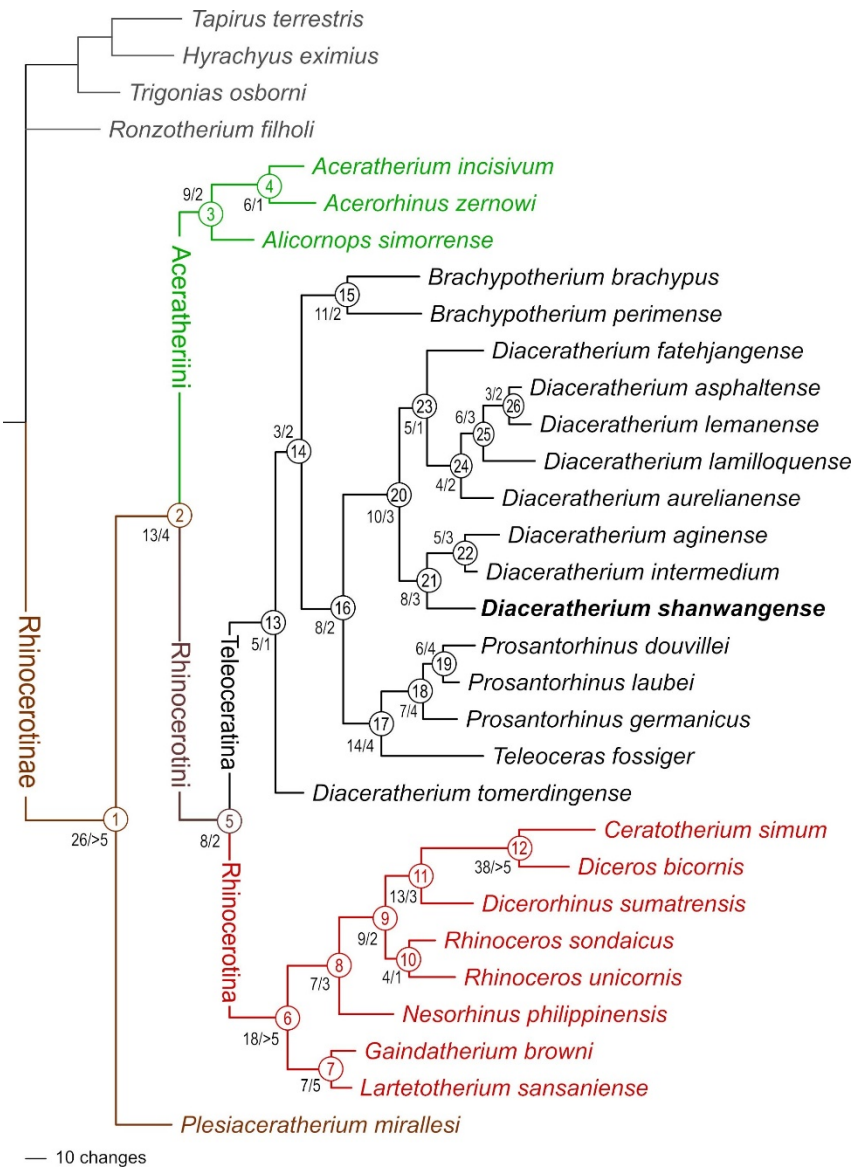

Fig. 11. Phylogram of Rhinocerotinae, with a focus on Teleoceratina. Most parsimonious tree (1315 steps; consistency index = 0.2700; retention index = 0.4923), retrieved from 282 unweighted cranio-mandibular, dental, and postcranial characters scored in 31 tapirid and rhinocerotoid species (see S1 and S2). Node numbers appear in empty circles. Number of unambiguous synapomorphies/Bremer Support are indicated left to nodes. [One column width suggested]

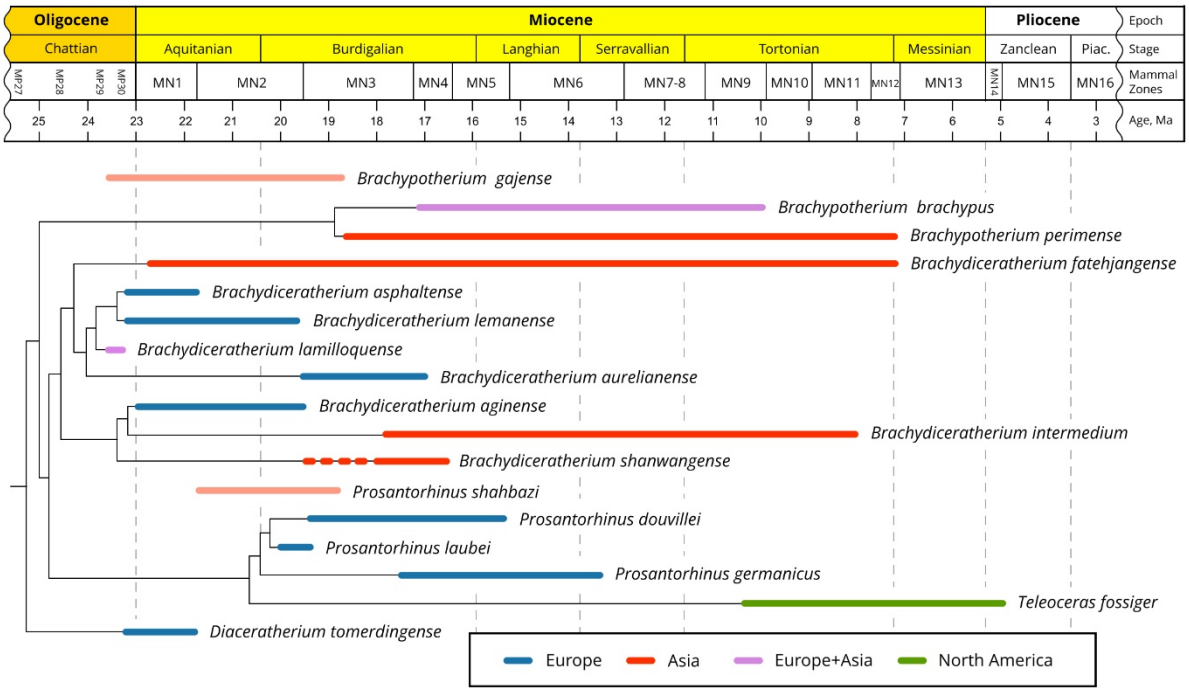

Fig. 12. Phylogenetic relationships of Teleoceratina versus time (see Fig. 11), with new combinations. Although they were not included in the current parsimony analysis, the temporal distributions of *Brachypotherium gajense* and *Prosantorhinus shahbazi* are provided here, as these species might bridge a stratigraphic gap for the concerned genera. [Full width suggested]

Fig. 13. Paleomap of Eurasia by early Miocene times (~20 Ma), showing the main occurrences of representatives of the teleoceratine rhinocerotid *Brachydiceratherium*, at the basin scale (apart from Tagay, Shanwang, and Nong Ya Plong localities). The Green area depicts the interpolated geographical range of *B. shanwangense* (with possible occurrences on Honshu Island, Japan). Based on data from Borissiak (1927), Cerdeño (1993), Antoine et al. (2000, 2013), Becker et al. (2009), Antoine & Becker (2013), Tomida et al. (2013), Jame et al. (2019), Handa (2020), Lu et al. (2021), Antoine (in press), and the present work. PalaeoAtlas by Scotese (2016, under cc 4.0 license) with added paleomap Baikal area (Mats et al., 2011). [Full width suggested]

Table 1. Distribution of unambiguous apomorphic characters (synapomorphies and autapomorphies, including reversals) among teleoceratine rhinocerotids, as retrieved in the current phylogenetic analysis. Node numbers match those of Fig. 11. Binominal combinations are as detailed in the Discussion.

Node 13 (Teleoceratina): -72^{0}, 129^{1}, 205^{1}, 279^{1}, 282^{1}

Diaceratherium tomerdingense (type and only species): -70^{0}, 90^{1}, 121^{1}, 130^{1}, -196^{0}, 212^{1}, 216^{1}, 223^{3}, 228^{2}, -251^{0}

Node 14: 199^{2}, 202^{1}, 227^{1}

Brachypotherium: -50^{0}, 54^{2}, -83^{1}, -114^{0}, 140^{1}, -146^{0}, 155^{1}, 203^{1}, 214^{1}, -226^{0}, 254^{1}

Brachypotherium brachypus: 3^{2}, -34^{0}, -39^{0}, 57^{1}, 62^{1}, 99^{2}, -109^{1}, -115^{2}, 118^{1}, -119^{0}, -135^{0}, 144^{1}, -149^{0}, 157^{3}, -159^{0}, -160^{0}, 170^{1}, 179^{1}, 180^{1}, 191^{1}, -193^{0}, -204^{0}, 209^{1}, 210^{1}, 239^{1}, 275^{2}, -280^{0}

Brachypotherium perimense: 25^{1}, 41^{1}, 68^{1}, 76^{1}, -85^{0}, 121^{1}, -125^{0}, 128^{1}, -129^{0}, 151^{3}, 172^{1}, 173^{1}, 175^{1}, 181^{1}, 199^{3}, 200^{1}, -205^{0}, 228^{2}, 246^{1}, 248^{1}, 255^{1}, 263^{3}, -271^{0}, 272^{1}, 274^{1}, 277^{1}, -282^{0}

Node 16: 38^{1}, 101^{1}, 107^{3}, -147^{0}, -222^{0}, -230^{0}, -263^{0}, 264^{3}

Node 17 (*Teleoceras* + *Prosantorhinus*): 10^{1}, 11^{1}, 40^{1}, 57^{1}, 95^{1}, 99^{1}, 130^{1}, 180^{1}, 190^{2}, 191^{1}, 234^{1}, 272^{2}, 275^{2}, -280^{0}

Teleoceras fossiger (type species): 2^{1}, 19^{1}, 25^{1}, 48^{1}, -56^{0}, 59^{1}, 60^{0}, 63^{1}, 68^{1}, 80^{1}, 87^{2}, 88^{2}, 91^{2}, 99^{2}, 102^{1}, 114^{3}, 116^{1}, 117^{1}, 121^{1}, 126^{1}, 128^{1}, 144^{1}, 151^{3}, 153^{1}, 157^{3}, 159^{3}, 165^{1}, 173^{1}, 175^{1}, 180^{3}, -196^{0}, 212^{1}, 220^{1}, 248^{1}, -249^{0}, 254^{1}, 268^{1}, 269^{1}, 276^{1}

Prosantorhinus: 1^{1}, 27^{1}, -35^{0}, 45^{1}, -119^{0}, -125^{0}, -177^{0}

Prosantorhinus germanicus (type species): 37^{1}, 85^{3}, 105^{1}, -109^{1}, -110^{0}, -111^{2}, 115^{2}, 147^{2}, 148^{1}, -149^{1}, -151^{1}, 166^{1}, -182^{0}

Node 19: -101^{0}, -129^{0}, -135^{0}, -159^{1}, 182^{2}, 261^{3}

Prosantorhinus laubei: -85^{1}, 90^{1}, -99^{0}, -114^{0}, -134^{0}, -180^{0}

Prosantorhinus douvillei: -88^{0}, 99^{2}, 114^{2}, 144^{1}, 156^{2}, -157^{0}, -159^{0}, 162^{1}, 180^{3}

Brachydiceratherium: -20^{0}, -39^{0}, 65^{1}, 101^{3}, -149^{1}, -159^{0}, 185^{1}, 187^{2}, 246^{1}, -251^{0}

Node 21: 72^{1}, 105^{2}, -190^{0}, -193^{0}, 238^{1}, 250^{1}, -279^{0}, -282^{0}

Brachydiceratherium shanwangense: 1^{1}, 27^{1}, 63^{1}, -70^{0}, -85^{0}, 87^{2}, 88^{2}, 105^{3}, 116^{1}, 147^{2}, 151^{3}, 157^{3}, 191^{1}, -196^{0}, 199^{3}, 234^{1}

Node 22: 121^{1}, 210^{1}, -252^{1}, -264^{0}, -265^{0}

Brachydiceratherium aginense: 112^{1}, -114^{0}, 128^{2}, 130^{1}, -149^{0}, 162^{1}, 214^{1}, 216^{1}, 219^{1}, -221^{0}, -226^{0}, 256^{1}, -262^{0}, 263^{1}, 272^{1}, -280^{0}

Brachydiceratherium intermedium: -65^{0}, 114^{3}, 118^{1}, -129^{0}, 220^{1}

Node 23: -119^{0}, 203^{1}, -204^{0}, 207^{1}, 261^{1}

Brachydiceratherium fatehjangense: 10^{1}, 18^{2}, 48^{1}, -49^{0}, 53^{1}, 54^{2}, 57^{1}, -70^{0}, -94^{1}, -107^{0}, 140^{1}, -149^{0}, 151^{3}, 155^{1}, 174^{1}, -202^{0}, -205^{0}, 209^{1}, -224^{0}, -227^{0}, -247^{0}, 261^{2}

Node 24: 118^{1}, -125^{0}, -134^{0}, 230^{1}

Brachydiceratherium aurelianense: -53^{0}, 86^{1}, 90^{3}, 114^{3}, 124^{1}, 130^{1}, 147^{1}, -193^{0}, 198^{1}, -199^{0}, 214^{1}, 220^{1}

Node 25: 105^{1}, 210^{1}, -253^{0}, -264^{0}, -279^{0}, -280^{0}

Brachydiceratherium lamilloquense: 53^{2}, -84^{1}, 88^{1}, 99^{1}, -102^{1}, 105^{3}, -111^{2}, 112^{3}, -135^{0}, -146^{0}, 207^{2}, 228^{2}, -243^{0}, -246^{0}, -247^{0}, 248^{1}, -259^{0}

Node 26: -109^{0}, -138^{0}, -221^{0}

Brachydiceratherium asphaltense: -23^{0}, 27^{1}, 83^{3}, -227^{0}

Brachydiceratherium lemanense (type species): 11^{1}, 40^{1}, 45^{1}, -47^{0}, 48^{1}, -50^{0}, -70^{0}, 147^{1}, -226^{1}